iScience

CellPress
OPEN ACCESS

Article

Mevalonate biosynthesis pathway regulates the development and survival of brown adipocytes

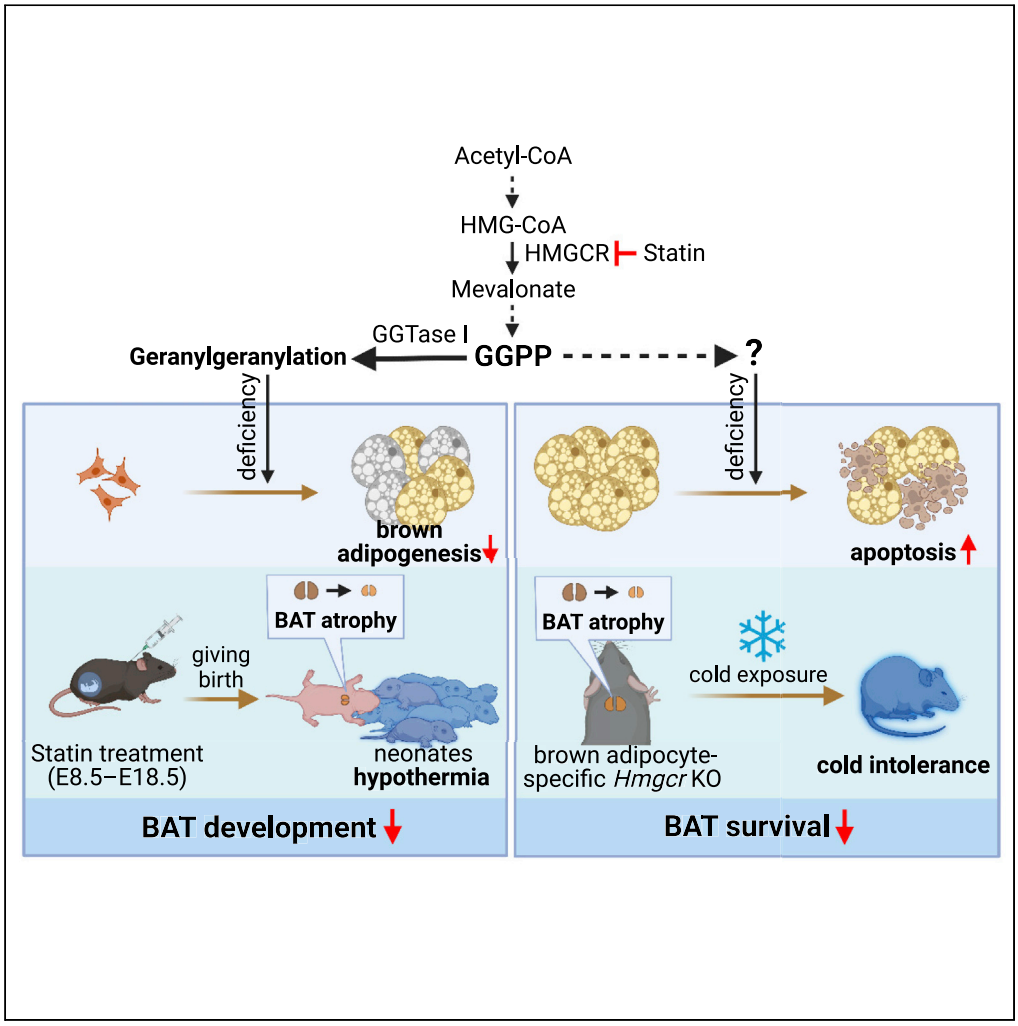

Jungin Kwon, Yu-Sheng Yeh, Satoko Kawarasaki, ..., Kazuo Inoue, Teruo Kawada, Tsuyoshi Goto

goto.tsuyoshi.6x@kyoto-u.ac.jp

Highlights

Protein geranylgeranylation is essential for brown adipocyte differentiation

Neonates exposed to statin during the embryonic period exhibit BAT atrophy

GGPP is required for survival of mature brown adipocytes

Brown adipocyte-specific *Hmgcr*-deficient mice show BAT atrophy

Kwon et al., iScience 26, 106161
March 17, 2023
https://doi.org/10.1016/j.isci.2023.106161

iScience

CellPress
OPEN ACCESS

Article

Mevalonate biosynthesis pathway regulates the development and survival of brown adipocytes

Jungin Kwon,[1] Yu-Sheng Yeh,[1] Satoko Kawarasaki,[1] Hiroto Minamino,[2] Yoshihito Fujita,[2] Yuko Okamatsu-Ogura,[3] Haruya Takahashi,[1] Wataru Nomura,[1,4] Shigenobu Matsumura,[5] Rina Yu,[6] Kazuhiro Kimura,[3] Masayuki Saito,[3] Nobuya Inagaki,[2] Kazuo Inoue,[1,4] Teruo Kawada,[1,4] and Tsuyoshi Goto[1,4,7,*]

SUMMARY

The high thermogenic activity of brown adipose tissue (BAT) has received considerable attention. Here, we demonstrated the role of the mevalonate (MVA) biosynthesis pathway in the regulation of brown adipocyte development and survival. The inhibition of 3-hydroxy-3-methylglutaryl-CoA reductase (HMGCR), the rate-limiting enzyme in the MVA pathway and the molecular target of statins, suppressed brown adipocyte differentiation by suppressing protein geranylgeranylation-mediated mitotic clonal expansion. The development of BAT in neonatal mice exposed to statins during the fetal period was severely impaired. Moreover, statin-induced geranylgeranyl pyrophosphate (GGPP) deficiency led to the apoptosis of mature brown adipocytes. Brown adipocyte-specific *Hmgcr* knockout induced BAT atrophy and disrupted thermogenesis. Importantly, both genetic and pharmacological inhibition of HMGCR in adult mice induced morphological changes in BAT accompanied by an increase in apoptosis, and statin-treated diabetic mice showed worsened hyperglycemia. These findings revealed that MVA pathway-generated GGPP is indispensable for BAT development and survival.

INTRODUCTION

Obesity is a major risk factor for type 2 diabetes (T2D)[1,2] and is characterized by excessive accumulation of adipose tissue, which is composed of white adipose tissue (WAT) and brown adipose tissue (BAT). Unlike WAT, which stores excessive energy in the form of triglycerides, BAT oxidizes energy substrates such as fats, carbohydrates, and branched-chain amino acids to produce heat via mitochondrial uncoupling protein 1 (UCP1); therefore, BAT is considered a metabolically active tissue.[3–6] Notably, rodent and human studies have shown that BAT activity is inversely correlated with adiposity and insulin resistance.[5,7–9] Moreover, a previous study indicated that individuals with BAT have a significantly lower prevalence of T2D.[10] Thus, increasing the quantity or quality of BAT could be a promising therapeutic strategy for obesity and T2D.

The mevalonate (MVA) biosynthesis pathway produces both sterols and non-sterols.[11] Among non-sterols, isoprenoids, such as farnesyl pyrophosphate (FPP) and geranylgeranyl pyrophosphate (GGPP), play pivotal roles in the post-translational modification (prenylation) of Ras and Ras-related small GTP-binding proteins and in the formation of biologically important molecules, including coenzyme Q,[11] thereby regulating several cellular processes.[12] Statins, which are inhibitors of 3-hydroxy-3-methylglutaryl-CoA reductase (HMGCR), a rate-limiting enzyme in the MVA pathway, are widely used for the clinical management of hypercholesterolemia. Along with the low-density lipoprotein cholesterol-lowering effect, statins can exhibit multiple pleiotropic effects that confer protection against cardiovascular diseases.[13] However, statins also exhibit several adverse effects, such as rhabdomyolysis, liver damage, and an increased risk of T2D, which appear to be primarily mediated by the suppression of isoprenoid biosynthesis.[14] Although the mechanisms underlying the adverse effects on skeletal muscle and the liver have been gradually clarified by tissue-specific inhibition of the MVA pathway in mice,[15–17] the mechanisms underlying the statin-mediated increased risk of T2D remain unclear. A recent study showed an inverse correlation between statin use and active BAT in humans.[10,18] BAT dysfunction owing to inhibition of the MVA pathway could be associated with an increased risk of T2D following statin use.

[1]Division of Food Science and Biotechnology, Graduate School of Agriculture, Kyoto University, Kyoto 611-0011, Japan

[2]Department of Diabetes, Endocrinology, and Nutrition, Graduate School of Medicine, Kyoto University, Kyoto 606-8507, Japan

[3]Departments of Basic Veterinary Sciences, Faculty of Veterinary Medicine, Hokkaido University, Sapporo 060-0818, Japan

[4]Research Unit for Physiological Chemistry, the Center for the Promotion of Interdisciplinary Education and Research, Kyoto University, Kyoto 606-8501, Japan

[5]Division of Clinical Nutrition, Graduate School of Comprehensive Rehabilitation, Osaka Prefecture University, Osaka 583-0872, Japan

[6]Department of Food Science and Nutrition, University of Ulsan, Ulsan 44610, Republic of Korea

[7]Lead contact

*Correspondence: goto.tsuyoshi.6x@kyoto-u.ac.jp

https://doi.org/10.1016/j.isci.2023.106161

The number of adipocytes is thought to be defined by the balance between newly differentiated adipocytes from preadipocytes and dead adipocytes. Upon hormonal induction of differentiation, growth-arrested preadipocytes re-enter the cell cycle and undergo several rounds of mitosis, which is referred to as mitotic clonal expansion (MCE).[19,20] Transcription factors C/EBPβ and C/EBPδ, members of the CCAAT/enhancer-binding protein (C/EBP) family, are involved in the initiation of the clonal expansion phase.[21,22] C/EBPβ and C/EBPδ interact with C/EBP regulatory elements to activate the transcription of adipocyte-specific genes, including peroxisome proliferator-activated receptor gamma (*Pparg*) and *Cebpa*, which are master transcription factors of adipogenesis.[23,24] Differentiated adipocytes meet their fate via apoptosis, where activated caspase 3 induces cell death.[25] Under normal physiological conditions, adipocyte number seems constant, and approximately 10% of fat cells undergo annual turnover in adults.[26] Conditions such as intake of a high-fat diet and PPARγ agonist treatment, which are known to increase adipogenesis, have been found to be associated with increased adipocyte death.[27,28] These studies indicate that adipogenesis and adipocyte death are mutually controlled and are crucial regulatory events for maintaining adipose tissue mass. Dysregulation of either brown adipogenesis or brown adipocyte death can lead to abnormal regulation of BAT mass.[29–31] BAT atrophy leads to impaired thermogenesis and glucose intolerance.[32,33] These findings indicate that brown adipogenesis and brown adipocyte death play pivotal roles in maintaining BAT mass and function.

Although the essential role of the MVA pathway in adipocyte browning, which is a process converting white adipocytes to thermogenic adipocytes, has been reported,[18] the detailed physiological roles of the MVA pathway in brown adipogenesis and brown adipocyte survival and their underlying mechanisms remain largely unknown. In the present study, we demonstrated that the MVA pathway–mediated GGPP production is required for both brown adipogenesis and brown adipocyte survival, which subsequently affects BAT function. Our findings revealed that GGPP is an essential regulatory factor for BAT mass and function.

RESULTS

Hmgcr expression levels are highly correlated with *Ucp1* expression levels in BAT and brown adipocytes

As shown in Figure 1A, mRNA expression levels of *Hmgcr* were found to be high in the testis and brain, which is consistent with a previous study.[34] *Hmgcr* mRNA expression levels in BAT are similar to those in skeletal muscles, in which HMGCR has been reported to be functional.[17] Because the thermogenic function of BAT is upregulated under cold temperatures, we examined HMGCR expression levels during cold exposure. Interestingly, mRNA and protein expression levels of HMGCR were increased by cold exposure. Although mRNA expression of *Hmgcr* was immediately induced (~8 h) (Figure 1B), prolonged cold exposure was required to markedly increase its protein levels (~48 h) (Figure 1D). Both HMGCR mRNA and protein expression patterns were highly correlated with those of *UCP1*, the gene responsible for non-shivering thermogenesis in brown adipocytes (Figures 1C and 1E). To investigate whether cold-induced β-adrenergic stimulation was involved in the upregulation of *Hmgcr* mRNA expression in brown adipocytes, the effect of isoproterenol (ISO), a β-adrenergic receptor agonist, on *Hmgcr* expression in HB2 brown adipocytes was examined. Similar to *Ucp1*, *Hmgcr* expression was markedly induced by ISO treatment (Figures 1F and S1A). We confirmed that *Hmgcr* expression was closely associated with the expression of *Ucp1* in brown adipocytes during β-adrenergic stimulation (Figures 1G and S1B). Moreover, HMGCR protein exhibited a similar expression pattern as UCP1 protein, peaking at 12 h in response to ISO stimulation (Figure S1C), which showed a strong positive correlation (Figure S1D). These findings indicate that *Hmgcr* expression in brown adipocytes is highly associated with *Ucp1* expression, which raises the possibility that the MVA pathway plays an important role in regulating BAT function.

Inhibition of the MVA biosynthesis pathway by statins impairs the differentiation capacity of HB2 brown preadipocytes

First, we determined the mRNA expression level of *Hmgcr* in HB2 cells. *Hmgcr* was highly expressed in HB2 brown preadipocytes and gradually decreased in differentiated HB2 cells, in which adiponectin (*Adipoq*) was highly expressed (Figure S2). Based on these results, HB2 brown preadipocytes were induced to differentiate in the presence of statins to investigate the potential role of the MVA pathway in brown adipocyte differentiation. Treatment with statins (atorvastatin [ATR] and lovastatin [LVS]) in the early stages of brown adipocyte differentiation suppressed lipid accumulation in a dose-dependent manner (Figures 2A and 2B). Moreover, LVS treatment suppressed the expression of adipocyte marker genes, including *Pparg*, fatty acid–binding protein 4 (*Fabp4*), and *Adipoq*, accompanied by marked suppression of *Ucp1* (Figure 2C).

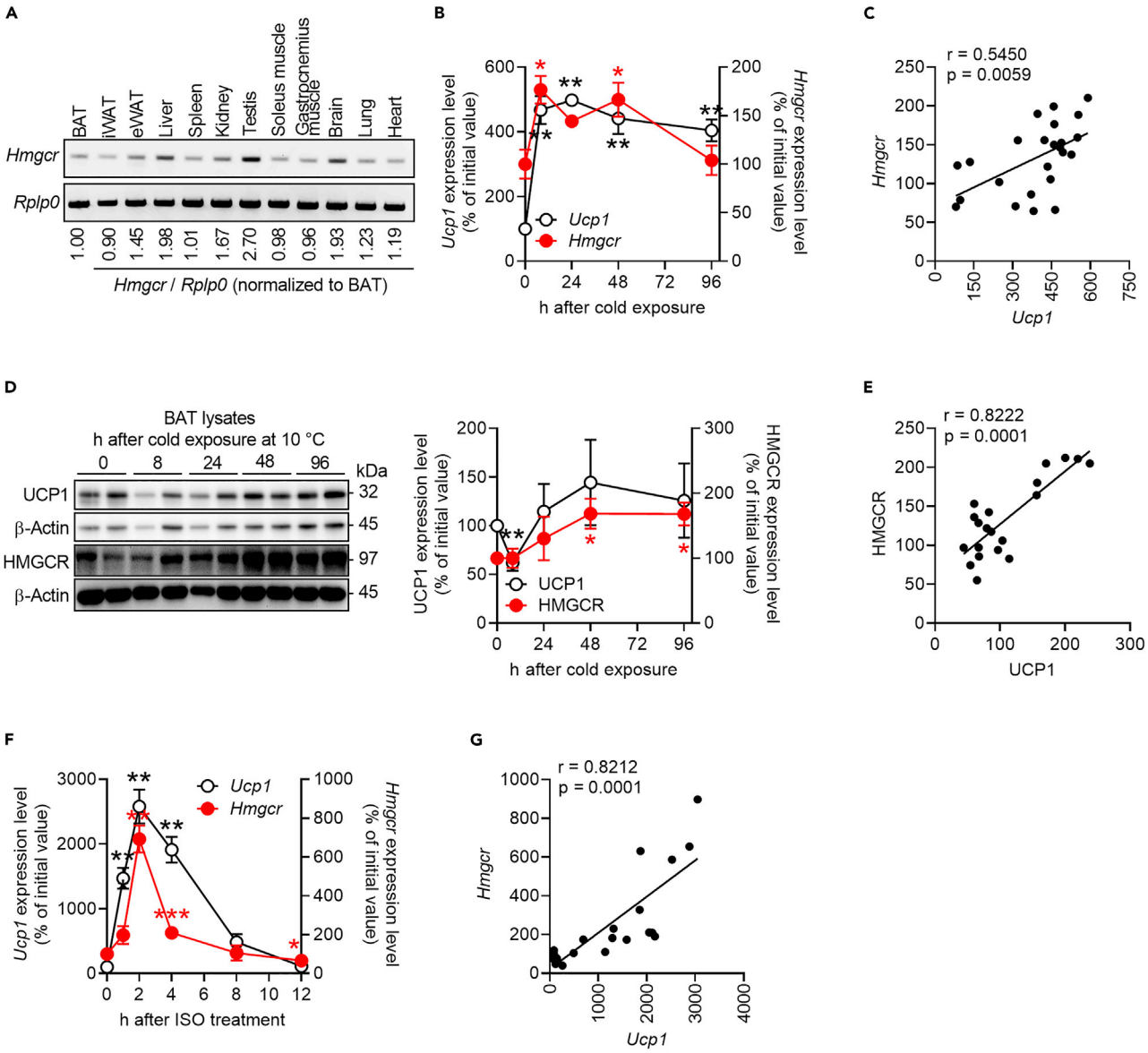

Figure 1. *Hmgcr* expression levels highly correlate with *Ucp1* expression levels in BAT and brown adipocytes

(A) *Hmgcr* mRNA levels in various tissues from 8-week-old male C57BL/6J mice (n = 2).

(B) mRNA levels of *Ucp1* and *Hmgcr* in BAT of 14-week-old male C57BL/6N mice exposed to cold at 10°C for an indicated time period (n = 4–8).

(C) Correlation between *Ucp1* and *Hmgcr* analyzed based on data from (B).

(D) Representative immunoblots of UCP1 and HMGCR (left) and relative protein abundance (right; n = 4). Each protein level was normalized to β-Actin.

(E) Correlation between UCP1 and HMGCR analyzed based on data from (D).

(F) mRNA levels of *Ucp1* and *Hmgcr* in HB2 cells after 1-μM isoproterenol (ISO) treatment (n = 3–4).

(G) Correlation between *Ucp1* and *Hmgcr* analyzed based on data from (F). Data are shown as the mean ± SEM. *p < 0.05, **p < 0.01, ***p < 0.001 by unpaired two-tailed Student's *t* test. Correlation was analyzed by Pearson's correlation. Black asterisk: vs. initial value of Ucp1; Red asterisk: vs. initial value of Hmgcr. iWAT, inguinal white adipose tissue; eWAT, epididymal white adipose tissue. See also Figure S1.

Notably, statin treatment suppressed the adipogenic stimulation-induced increase in DNA content (Figures 2A and 2D), suggesting that HMGCR suppression inhibited MCE during brown adipogenesis. Time-course experiment showed that differentiation induction of brown preadipocytes increased DNA content by almost 2.2 times 48 h after differentiation induction, whereas only 1.6 times increase in DNA content was observed in the presence of LVS (Figure 2E). These findings indicated that the MVA pathway is required for adequate MCE during brown adipocyte differentiation.

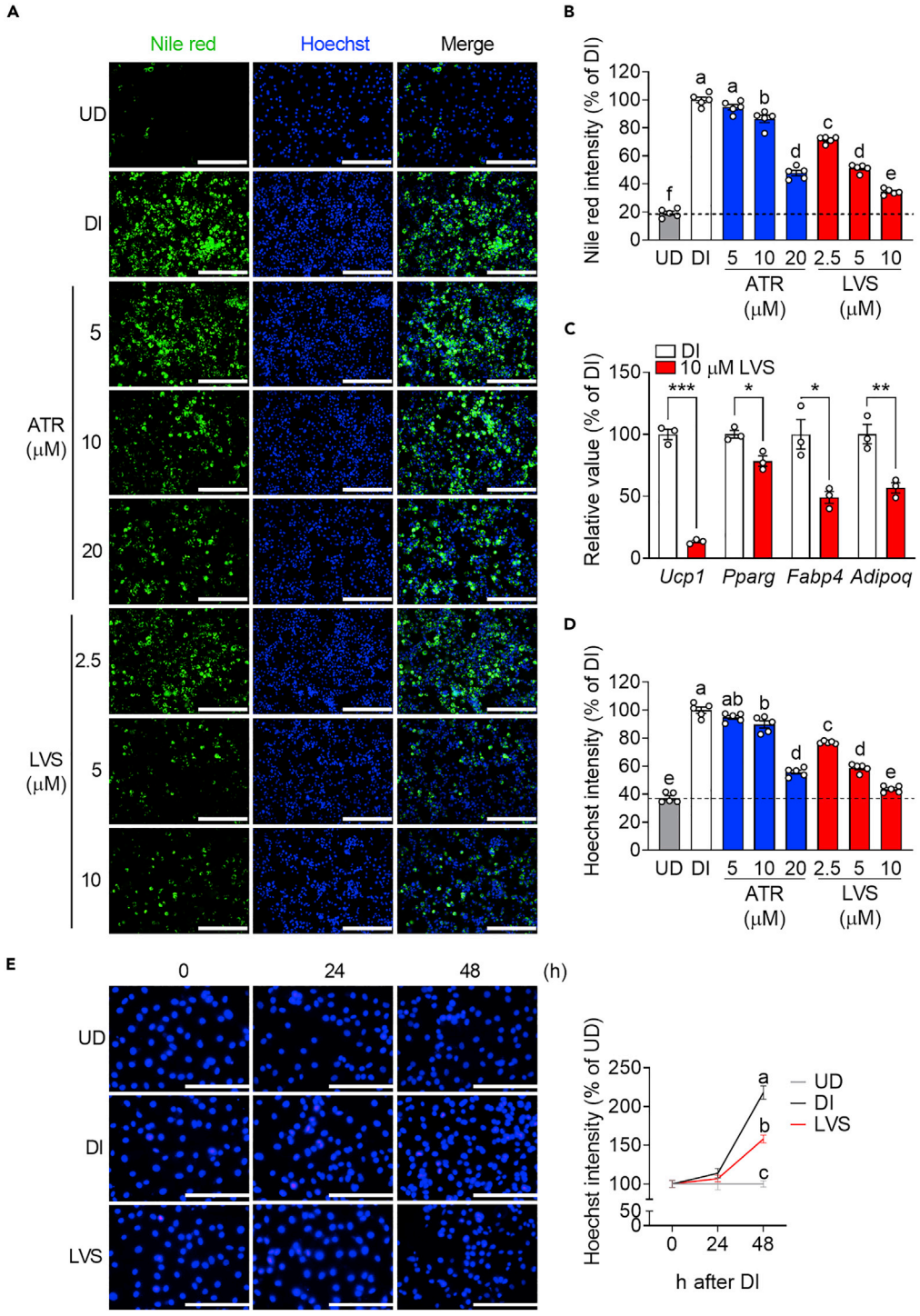

Figure 2. Inhibition of the MVA biosynthesis pathway by statins impairs the differentiation capacity of HB2 brown preadipocytes

(A) Representative microscopic view of undifferentiated (UD), differentiation-induced (DI), ATR-treated (days 0–2), or LVS-treated (days 0–2) HB2 cells after staining with Nile red (left) and Hoechst (middle) on day 4, respectively. Scale bars, 300 μm.

(B) Relative fluorescence intensity of Nile red (n = 5).

(C) Relative mRNA levels in HB2 cells treated with or without 10-μM LVS (days 0–2) on day 4 (n = 3).

(D) Relative fluorescence intensity of Hoechst staining (n = 5).

Figure 2. *Continued*

(E) Representative microscopic view of UD, DI, or 10-μM LVS-treated HB2 cells after staining with Hoechst at indicated time points (left) and relative fluorescence intensity of Hoechst (right; n = 5–6). Scale bars, 200 μm. Data are shown as the mean ± SEM. *p < 0.05, **p < 0.01, ***p < 0.001 by unpaired two-tailed Student's *t* test for (C). Groups with different letters are significantly different (p < 0.05) as determined by one-way ANOVA with Tukey's honestly significant difference (HSD) post-hoc analysis for (B), (D), and (E). See also Figure S2.

Protein geranylgeranylation is required for HB2 cell differentiation

To determine the metabolites responsible for the regulation of brown adipogenesis in the MVA pathway, HB2 cells were treated with LVS in combination with or without MVA, FPP, GGPP, or squalene (SQ) (Figure 3A). We found that LVS-induced inhibition of brown adipogenesis was largely recovered by MVA or GGPP (Figure 3B). Analysis of the fluorescence intensity of Nile red–stained cells revealed that the suppressed lipid accumulation by LVS treatment was partially recovered by MVA or FPP and completely recovered by GGPP co-treatment (Figure 3C). Moreover, LVS-induced suppression of differentiation-induction-activated cell proliferation was completely abolished in the presence of MVA or GGPP but not by FPP or SQ (Figure 3D). Consistent with the phenotypic results, LVS-induced suppression of the mRNA expression levels of *Ucp1* and adipocyte marker genes, such as *Fabp4* and *Adipoq*, was largely recovered by co-treatment with GGPP in HB2 brown adipocytes (Figure 3E). The time-course experiment clearly showed that GGPP co-treatment allowed HB2 cells to undergo MCE, as shown by the increase in DNA content to the same extent level as that in differentiation-induced (DI) HB2 cells (Figure 3F). Because LVS treatment at the concentrations used in this study has been reported to suppress cellular GGPP levels,[35,36] these findings clearly indicated that the MVA pathway–mediated GGPP production is essential for MCE during brown adipocyte differentiation. To further confirm whether GGPP is the key metabolite for brown adipocyte differentiation, HB2 cells were treated with zoledronate (Zol), a nitrogen-containing bisphosphonate, to inhibit geranylgeranyl pyrophosphate synthase 1, which is required for GGPP biosynthesis.[37] Although Zol treatment at the beginning of brown adipogenesis significantly decreased intracellular lipid accumulation (Figures 3G and 3H; DI 100.0 ± 5.8 vs. Zol 47.3 ± 4.0, p = 0.0000) and DNA content (Figures 3G and 3I; DI 100.0 ± 3.6 vs. Zol 61.9 ± 2.4, p = 0.0000), these effects were completely reversed by co-treatment with GGPP (Figures 3G–3I). Coenzyme Q_{10}, a product of GGPP, has been shown to be important for BAT function[38]; however, co-treatment with coenzyme Q_{10} (ubiquinol [$CoQH_2$; reduced form] or ubiquinone [CoQ; oxidized form]) could not recover either LVS-induced suppression of lipid accumulation (Figures 3J, 3K, S3A, and S3B) or LVS-induced suppression of the increase in DNA content (Figures 3L, 3M, S3A, and S3B), suggesting that LVS-mediated suppression of coenzyme Q_{10} production is not important for the anti-brown adipogenic effects of LVS. The attachment of GGPP to a target protein, called protein geranylgeranylation, is catalyzed by geranylgeranyltransferase type 1 (GGTase I).[39] To investigate the effect of protein geranylgeranylation, GGTI-286, a GGTase I inhibitor, was used at the beginning of brown adipocyte differentiation. Similar to the effects of LVS, treatment with more than 10 μM of GGTI-286 significantly suppressed both lipid accumulation and increased DNA content (Figures 3N and 3O). Although co-treatment with GGPP significantly recovered GGTI-286-induced suppression of lipid accumulation (Figures 3P and 3Q; GGTI-286 + GGPP 60.8 ± 1.7 vs. GGTI-286 48.4 ± 1.2, p = 0.0022; vs. DI 100.0 ± 2.5, p = 0.0000) and cell proliferation (Figures 3P and 3R; GGTI-286 + GGPP 65.2 ± 2.4 vs. GGTI-286 50.5 ± 1.5, p = 0.0039; vs. DI 100.0 ± 3.2, p = 0.0000), these recoveries were very limited. These results indicated that GGPP-mediated protein geranylgeranylation is essential for adequate MCE in differentiating brown adipocytes.

Neonates exposed to LVS during the BAT developmental period exhibit BAT atrophy and fail to maintain body temperature

Previous reports have shown that BAT develops from embryonic day 10 (E10) to postnatal day 2 (P2)[40]; thus, we administered LVS to pregnant dams to expose their fetuses to LVS from E8.5 to E18.5, as shown in Figure 4A. Notably, neonates from the LVS-injected dam showed interscapular BAT atrophy (Figures 4B and 4C). The BAT weight normalized to body weight yielded similar results (Figure 4D). Experiments using UCP1- monomeric red fluorescent protein 1 (mRFP1) reporter mice[41] showed that LVS exposure during the embryonic period significantly reduced mRFP1-derived fluorescence in the interscapular region, suggesting that UCP1 expression levels in BAT are suppressed by LVS (Figures 4E and 4F; vehicle (Veh) 100.0 ± 5.7 vs. LVS 78.4 ± 7.8, p = 0.0399). Actually, the surface temperature of neonates exposed to LVS was significantly lower than that of Veh-exposed neonates (Figure 4G; Veh 28.44°C ± 0.28 vs. LVS 26.02°C ± 0.48, p = 0.0001). A histochemical analysis showed that LVS-exposed neonatal BAT barely consisted of adipocytes with lipid droplets compared with Veh-exposed BAT (Figure 4H). Consistent with this, LVS treatment decreased the number of monocarboxylate transporter isoform 1 (a marker for mature brown

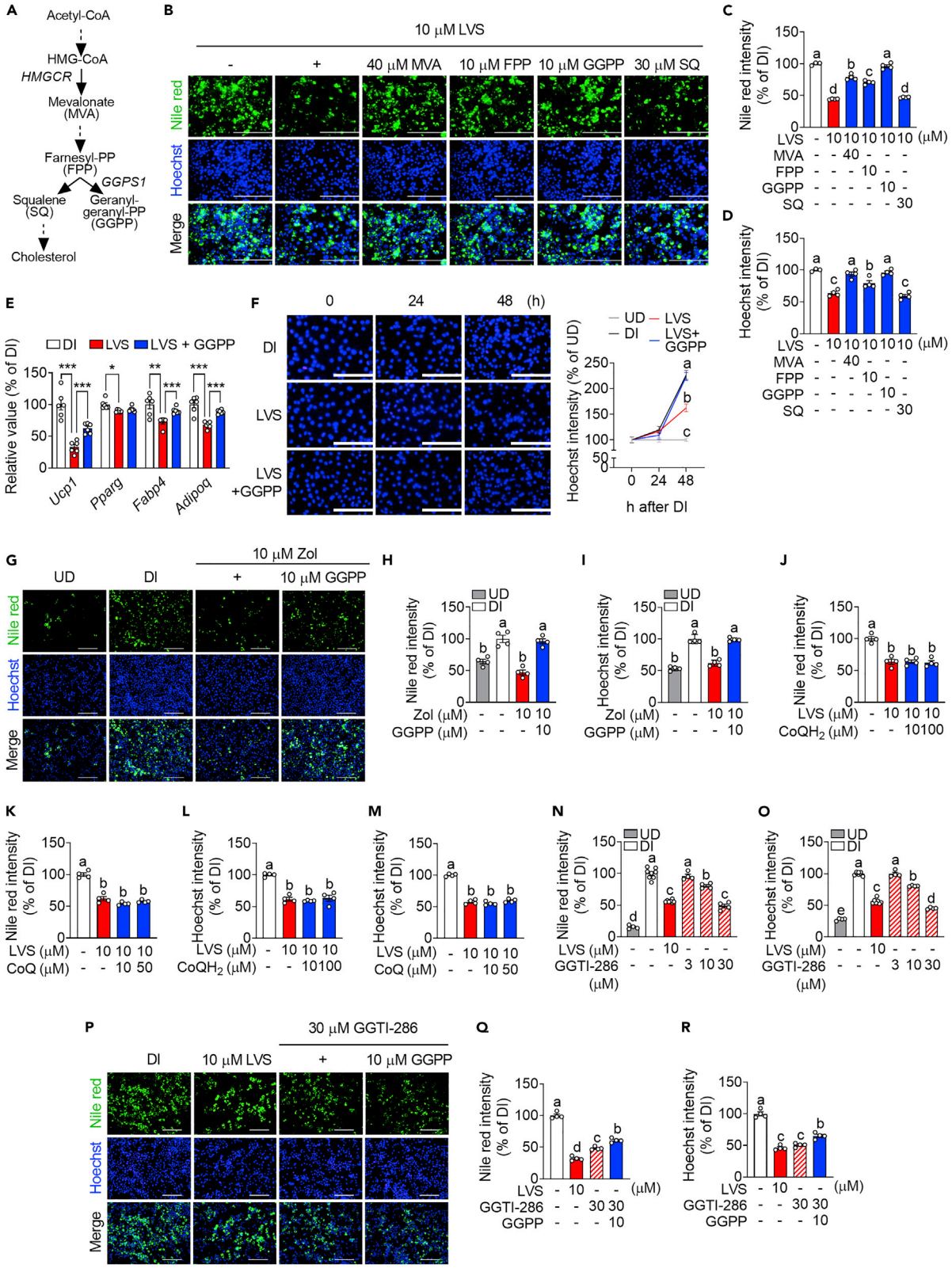
A
Acetyl-CoA
HMG-CoA
HMGCR
Mevalonate (MVA)
Farnesyl-PP (FPP)
GGPS1
Squalene (SQ)
Geranyl-geranyl-PP (GGPP)
Cholesterol
B
10 μM LVS
-
+
40 μM MVA
10 μM FPP
10 μM GGPP
30 μM SQ
Nile red
Hoechst
Merge
C
Nile red intensity (% of DI)
LVS - 10 10 10 10 10 (μM)
MVA - - 40 - - -
FPP - - - 10 - -
GGPP - - - - 10 -
SQ - - - - - 30
D
Hoechst intensity (% of DI)
LVS - 10 10 10 10 10 (μM)
MVA - - 40 - - -
FPP - - - 10 - -
GGPP - - - - 10 -
SQ - - - - - 30
E
DI
LVS
LVS + GGPP
Relative value (% of DI)
Ucp1
Pparg
Fabp4
Adipoq
F
0
24
48 (h)
DI
LVS
LVS +GGPP
UD
DI
LVS
LVS+ GGPP
Hoechst intensity (% of UD)
h after DI
G
10 μM Zol
UD
DI
+
10 μM GGPP
Nile red
Hoechst
Merge
H
Nile red intensity (% of DI)
Zol (μM) - - 10 10
GGPP (μM) - - - 10
I
Hoechst intensity (% of DI)
Zol (μM) - - 10 10
GGPP (μM) - - - 10
J
Nile red intensity (% of DI)
LVS (μM) - 10 10 10
CoQH2 (μM) - - 10 100
K
Nile red intensity (% of DI)
LVS (μM) - 10 10 10
CoQ (μM) - - 10 50
L
Hoechst intensity (% of DI)
LVS (μM) - 10 10 10
CoQH2 (μM) - - 10 100
M
Hoechst intensity (% of DI)
LVS (μM) - 10 10 10
CoQ (μM) - - 10 50
N
Nile red intensity (% of DI)
LVS (μM) - - 10 - - -
GGTI-286 (μM) - - - 3 10 30
O
Hoechst intensity (% of DI)
LVS (μM) - - 10 - - -
GGTI-286 (μM) - - - 3 10 30
P
30 μM GGTI-286
DI
10 μM LVS
+
10 μM GGPP
Nile red
Hoechst
Merge
Q
Nile red intensity (% of DI)
LVS - 10 - - (μM)
GGTI-286 - - 30 30
GGPP - - - 10
R
Hoechst intensity (% of DI)
LVS - 10 - - (μM)
GGTI-286 - - 30 30
GGPP - - - 10

Figure 3. Protein geranylgeranylation is required for HB2 cell differentiation

(A) Schematic overview of the MVA pathway.

(B) Representative microscopic view of DI or LVS-treated HB2 cells with or without MVA, FPP, GGPP, or SQ treatment (days 0–2) after staining with Nile red (top) and Hoechst (middle) on day 4. Scale bars, 200 μm.

(C and D) Relative fluorescence intensities of Nile red (C) and Hoechst (D) staining (n = 3–4).

(E) Relative mRNA levels of DI, 10-μM LVS-treated, or 10-μM LVS plus 10-μM GGPP-treated (days 0–2) HB2 cells on day 4 (n = 6).

(F) Representative microscopic view of UD, DI, 10-μM LVS-treated, or 10-μM LVS plus 10-μM GGPP-treated HB2 cells after staining with Hoechst at the indicated time points (left) and relative fluorescence intensity of Hoechst (right; n = 5–8). Scale bars, 200 μm.

(G) Representative microscopic view of UD, DI, Zol-treated, or Zol plus GGPP-treated (days 0–2) cells after staining with Nile red (top) and Hoechst (middle) on day 4. Scale bars, 200 μm.

(H and I) Relative fluorescence intensity of Nile red (H) and Hoechst (I) staining (n = 4).

(J and K) Relative fluorescence intensity of Nile red staining of DI or LVS-treated HB2 cells with or without $CoQH_2$ (J; n = 4) or CoQ (K; n = 4) treatment (days 0–2) on day 4.

(L and M) Relative fluorescence intensity of Hoechst staining of DI or LVS-treated HB2 cells with or without $CoQH_2$ (L; n = 4) or CoQ (M; n = 4) treatment (days 0–2) on day 4.

(N and O) Relative fluorescence intensity of Nile red (N) and Hoechst (O) staining of UD, DI, LVS-treated, or GGTI-286-treated (days 0–2) HB2 cells on day 4 (n = 4–8).

(P) Representative microscopic view of DI, LVS-treated, or GGTI-286-treated HB2 cells with or without GGPP treatment (days 0–2) after staining with Nile red (top) and Hoechst (middle) on day 4. Scale bars, 200 μm.

(Q and R) Relative fluorescence intensity of Nile red (Q) and Hoechst (R) staining (n = 4). Data are shown as the mean ± SEM. *$p < 0.05$, **$p < 0.01$, ***$p < 0.001$ by unpaired two-tailed Student's *t* test for (E). Groups with different letters are significantly different ($p < 0.05$) as determined by one-way ANOVA with Tukey's HSD post-hoc analysis for (C), (D), (F), (H–O), (Q), and (R). See also Figure S3.

adipocytes[42])-positive cells, whereas the number of platelet-derived growth factor alpha (a marker for adipocyte progenitor cells[43])-positive cells increased in LVS-exposed BAT in immunofluorescence analysis (Figure 4I). Furthermore, both thermogenesis-related genes (*Ucp1*, PPARγ coactivator 1 alpha [*Pgc1a*], and PR domain containing 16 [*Prdm16*]) and adipocyte marker genes (*Pparg*, *Fabp4*, and *Adipoq*) in BAT were markedly downregulated by LVS treatment (Figure 4J). Further investigation was performed to determine the effects of fetal LVS exposure on the development of BAT in adult mice, following the schedule shown in Figure S4A. Fetal LVS exposure did not affect body weight or length, without significant changes in food intake (Figures S4B–S4D). Interestingly, BAT atrophy persisted even after the offspring from the LVS-exposed dam became adults, whereas other tissues and organs showed no apparent differences in weight compared to those of the offspring from the Veh-exposed dam (Figures S4E and S4F). However, obvious histological changes in BAT were not observed in fetal LVS-exposed BAT (Figure S4G). We also could not detect any changes in the mRNA expression levels of either thermogenesis-related genes (*Ucp1* and *Pgc1a*) or adipocyte marker genes (*Pparg*, *Fabp4*, and *Adipoq*) in BAT from a grown-up offspring of the LVS-exposed dam (Figure S4H). Consistently, no significant differences in UCP1 protein expression levels in BAT were observed between the Veh and LVS groups (Figure S4I). Taken together, these findings indicate that the MVA pathway in the embryonic period not only plays an essential role in the development of BAT in the fetus but also affects BAT mass in adult mice.

LVS-mediated suppression of retinoblastoma phosphorylation may be associated with the functional inactivation of C/EBPβ in HB2 cells

C/EBPβ and C/EBPδ are the main MCE regulators.[21,22] Although the mRNA expression of both *Cebpb* and *Cebpd* was induced soon after the induction of differentiation in HB2 brown preadipocytes, LVS treatment did not affect the expression of either gene (Figures 5A and 5B). However, we confirmed that LVS treatment decreased the ratio of nuclear to cytoplasmic C/EBPβ protein levels without affecting nuclear C/EBPδ protein levels (Figure S5) in differentiating HB2 cells (Figure 5C), suggesting that LVS treatment decreased the nuclear localization of C/EBPβ protein. Interestingly, total C/EBPβ protein levels were also suppressed by LVS treatment (Figure 5D), which is consistent with a previous report using white adipocytes.[44] A previous study showed that adipocyte differentiation stimuli-induced hyperphosphorylation of the retinoblastoma (RB) protein is required for the transcriptional activation of C/EBPβ in 3T3-L1 cells.[45] RB phosphorylation was strongly induced within a day by the induction of differentiation in HB2 cells, whereas it was barely detectable in the presence of LVS (Figure 5D). In fact, LVS treatment suppressed C/EBPβ target genes, which are known to be important transcription factors for terminal differentiation of brown adipocytes, such as *Pparg*, *Cebpa*, and sterol regulatory element binding protein 1c (*Srebp1c*), at 48 h after differentiation induction without affecting *Cebpb* expression levels (Figures 5E–5H). These findings suggest that LVS treatment suppresses RB phosphorylation, which is followed by a change in C/EBPβ nuclear localization and suppression of its transcriptional activation.

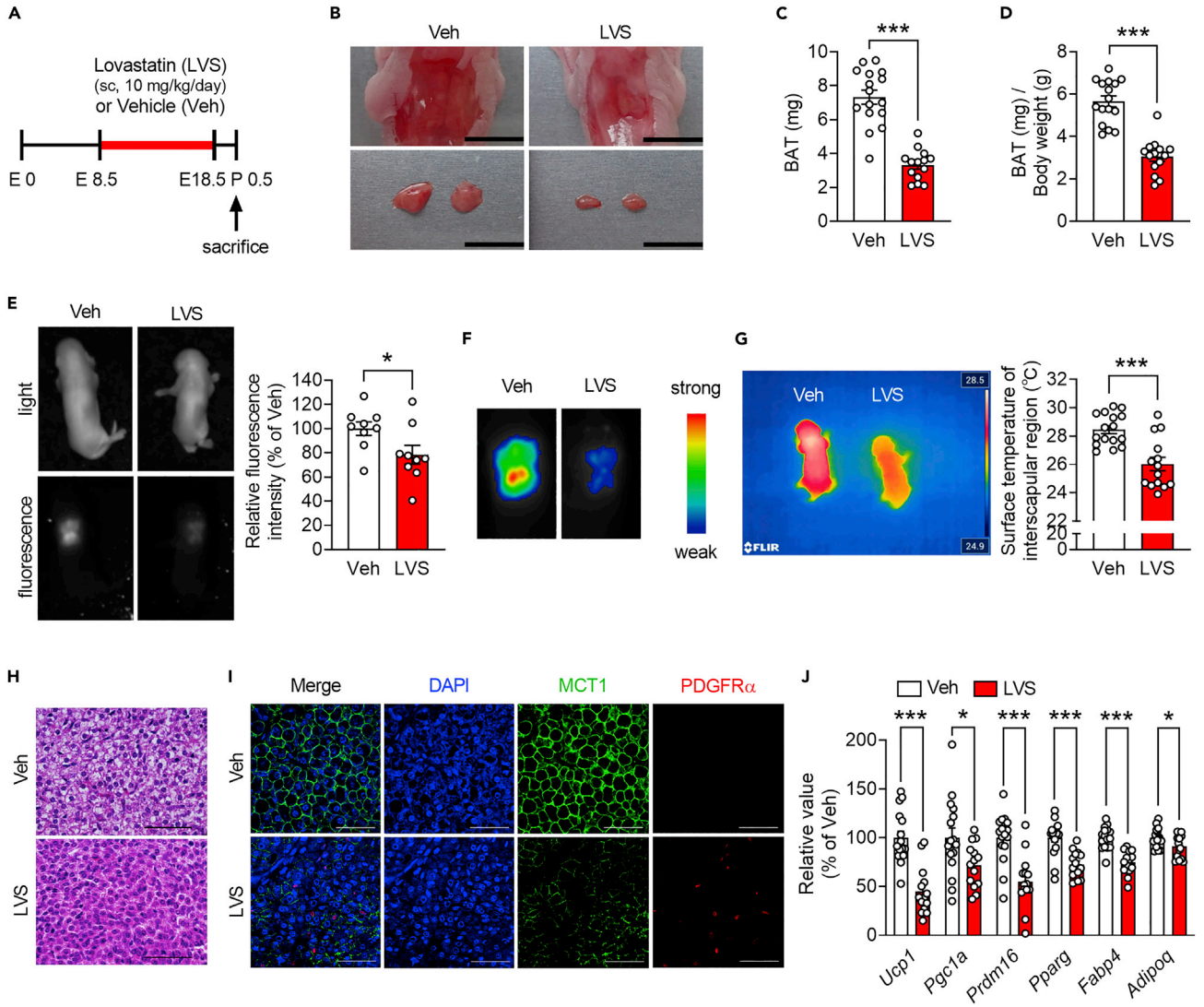

Figure 4. Neonates exposed to LVS during the BAT developmental period exhibit BAT atrophy and fail to maintain body temperature

(A) Schematic illustration of the *in vivo* LVS treatment experiment.

(B) Representative interscapular region (top) and BAT (bottom) images of neonates (P0.5). Scale bars, 1 cm.

(C and D) BAT weight (C) and BAT weight normalized to the body weight (D) of neonates (n = 14–16).

(E) *In vivo* imaging of prone-positioned UCP1-mRFP1 neonates (P0.5) in bright (left top) and fluorescent fields (left bottom) and relative fluorescence intensity around the interscapular area analyzed using ImageJ (right) (n = 9).

(F) Fluorescence intensity of the interscapular area of mice. The range of the surface plot represents 50–180 relative fluorescence units.

(G) Representative image of infrared thermography (left) and surface temperature of the interscapular region of neonates (P0.5) (right; n = 14–16).

(H) Representative images of hematoxylin and eosin (H&E)-stained BAT sections from neonates (P0.5). Scale bars, 50 μm.

(I) Representative immunofluorescence images of BAT isolated from neonates (P0.5). Scale bars, 40 μm.

(J) Relative mRNA levels in BAT isolated from neonates (P0.5) (n = 14–16). Data are shown as the mean ± SEM. *p < 0.05, ***p < 0.001 by unpaired two-tailed Student's *t* test. See also Figure S4.

GGPP recovers LVS-induced cell apoptosis in mature brown adipocytes

Next, we investigated the role of the MVA pathway in mature brown adipoytes. Differentiated HB2 brown adipocytes treated with LVS for 96 h showed a decrease in both lipid accumulation (Figures 6A and 6B) and Hoechst-stained nuclei (Figure 6A). The 3-(4,5-dimethylthiazol-2-yl)-5-(3-carboxymethoxyphenyl)-2-(4-sulfophenyl)-2H-tetrazolium (MTS) assay revealed that LVS treatment reduced the viability of HB2 brown adipocytes (Figure 6C), suggesting that reduced lipid accumulation and nuclear levels are derived from reduced cell viability. The LVS-induced reduction in lipid accumulation was almost completely recovered

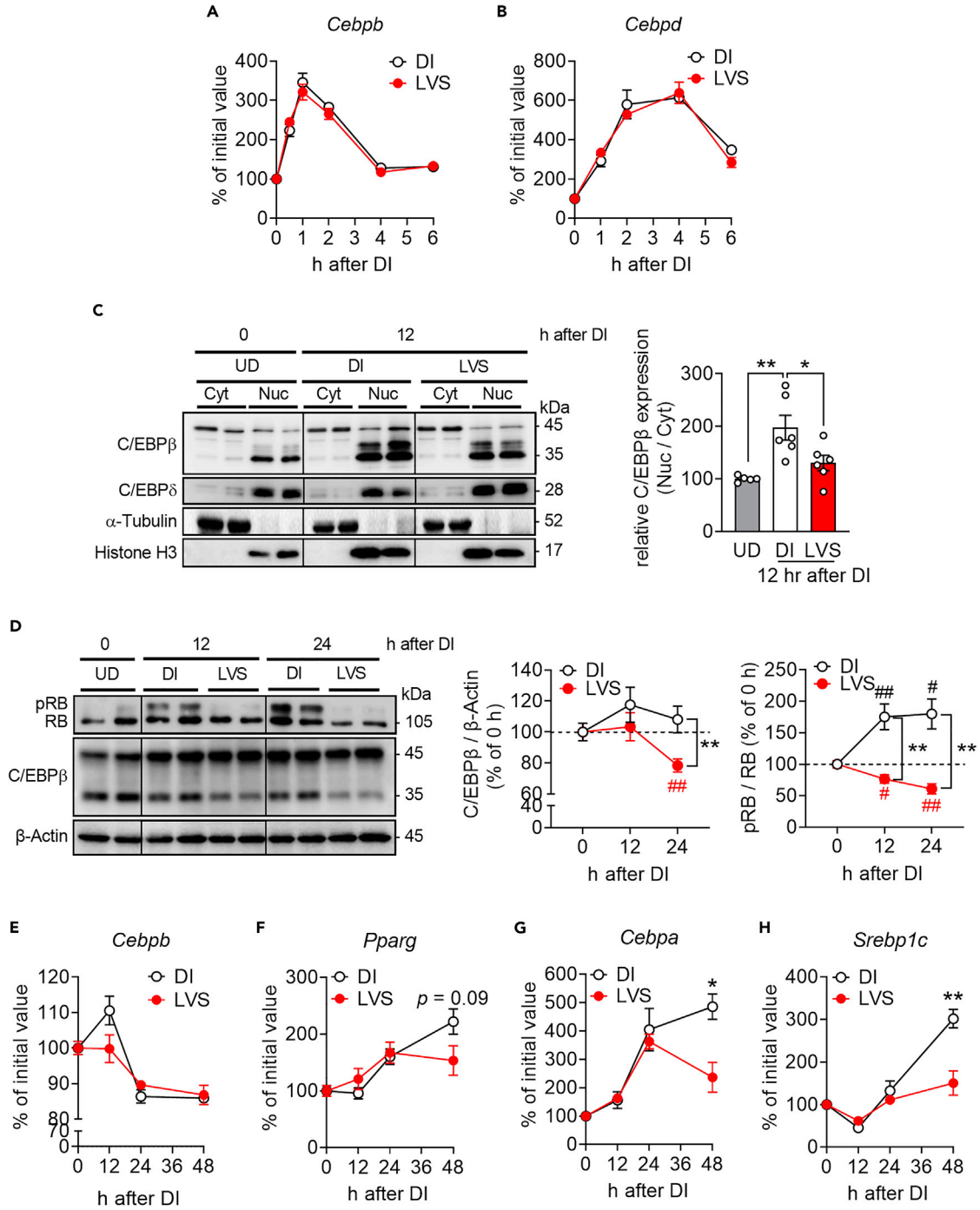

Figure 5. LVS-mediated suppression of retinoblastoma phosphorylation may be associated with the functional inactivation of C/EBPβ in HB2 cells

(A and B) Relative mRNA levels of *Cebpb* (A) and *Cebpd* (B) in differentiation-induced HB2 cells with or without 10-μM LVS treatment at the indicated time points (n = 3–8).

(C) Representative immunoblot of subcellular (Cyt, cytoplasm; Nuc, nucleus) expression of C/EBPβ and C/EBPδ in differentiation-induced HB2 cells with or without 10-μM LVS treatment at indicated time points (left). The band intensity of C/EBPβ was quantified using the ImageJ software. Nuclear C/EBPβ levels were normalized to cytoplasmic C/EBPβ levels (Nuc/Cyt) (right; n = 5–6). α-Tubulin, cytoplasmic fraction marker; Histone H3, nuclear fraction marker.

(D) Representative immunoblot of RB and C/EBPβ in differentiation-induced HB2 cells with or without 10-μM LVS treatment at the indicated time points. Phosphorylated RB (pRB) was determined by gel migrational difference (left). The band intensities of total C/EBPβ (middle), pRB, and RB (right) were quantified using the ImageJ software. C/EBPβ or pRB levels were normalized to β-Actin or total RB levels, respectively. C/EBPβ and pRB/RB levels at 0 h were arbitrarily set to 100 (n = 8).

Figure 5. *Continued*

(E–H) Relative mRNA levels of *Cebpb* (E), *Pparg* (F), *Cebpa* (G), and *Srebp1c* (H) in HB2 cells with or without 10-μM LVS treatment at the indicated time points (n = 3–6). Data are shown as the mean ± SEM. *p < 0.05, **p < 0.01, #p < 0.05, ##p < 0.01 by unpaired two-tailed Student's *t* test compared to UD or LVS-treated HB2 cells. Black sharp (#): vs. 0 h of DI; red sharp (#): vs. 0 h of LVS. See also Figure S5.

by co-treatment with MVA or GGPP (Figure 6B). FPP co-treatment also partially recovered lipid accumulation, whereas SQ co-treatment showed no recovery effect (Figure 6B). Consistent with the lipid accumulation levels, co-treatment with MVA or GGPP completely reversed the LVS-induced decrease in cell viability (Figure 6C). Next, we stained HB2 cells with an fluorescein isothiocyanate (FITC) -conjugated annexin V fluorescent probe and propidium iodide (PI), which stain cells in the early and late stages of apoptosis, respectively. As shown in Figure 6D, LVS treatment increased the number of both annexin V– and PI-stained HB2 brown adipocytes. The number of apoptotic cells was largely decreased by co-treatment with MVA or GGPP but not by co-treatment with FPP or SQ. Similar results were observed for the expression levels of the Bcl-2-associated X protein (*Bax*) and caspase 3 (*Casp3*), which are pro-apoptotic genes (Figure 6E). Moreover, cleaved-caspase 3 expression level, which represents the active form of caspase 3, was increased by treatment with LVS, whereas MVA or GGPP co-treatment almost reduced it in HB2 brown adipocytes (Figure 6F). These findings clearly indicate that the MVA pathway in brown adipocytes plays an essential role in survival of brown adipocytes by regulating apoptosis via GGPP production. Moreover, Zol treatment significantly decreased cell viability (DI 100.0 ± 4.8 vs. Zol 77.7 ± 6.0, p = 0.0499); however, this effect was almost reversed by co-treatment with GGPP (Figure 6G). Consistent with this, the increased *Bax* and *Casp3* expression levels after Zol treatment were completely abolished in the presence of GGPP (Figure 6H). However, co-treatment with coenzyme Q_{10} hardly prevented the LVS-induced decrease in viability of HB2 cells (Figures 6I and S6). Although 100-μM $CoQH_2$ treatment partially recovered the viability of LVS-treated HB2 cells (Figure 6I), the expression levels of pro-apoptotic markers remained unchanged (Figure 6J). To investigate the effect of protein geranylgeranylation, HB2 cells were treated with GGTI-286. We found that the inhibition of protein geranylgeranylation neither affected cell viability nor increased the expression levels of pro-apoptotic markers in HB2 cells (Figures 6K and 6L). These results indicate that GGPP plays an important role in the regulation of HB2 brown adipocyte survival through mechanisms other than coenzyme Q_{10} production and protein geranylgeranylation.

Brown adipocyte–specific *Hmgcr* knockout mice exhibit BAT atrophy and impaired thermoregulation

To validate the role of the MVA pathway in *Ucp1*-expressing mature brown adipocytes *in vivo*, we generated *Ucp1-Cre*-driven *Hmgcr* knockout (*Hmgcr*$^{flox/flox}$; *Ucp1-Cre*; BAT KO) mice. The *Hmgcr* knockout allele was observed only in the genomic DNA extracted from BAT but not in other tissues, including WATs, in BAT KO mice (Figure 7A). BAT KO mice grew normally until adulthood, and the body weight of BAT KO mice did not differ from that of *Hmgcr*$^{flox/flox}$ (control; Ctrl) mice (Figure 7B). However, the weight of interscapular BAT, unlike other tissues in BAT KO mice, was much lower than that in Ctrl mice, and its weight was only 28.6% of that of Ctrl mice (Figures 7C and 7D; Table S1). Histologically, BAT of BAT KO mice exhibited an extensive loss of adipocytes and a relative increase in non-lipid-laden cells (Figure 7E). We detected many cells undergoing apoptosis in BAT of BAT KO mice, as determined by an increase in terminal deoxynucleotidyl transferase–mediated deoxyuridine triphosphate (dUTP) nick end labeling (TUNEL)-positive cells. (Figure 7F). Histological analysis and TUNEL assay indicated that BAT atrophy observed in BAT KO mice was associated with the loss of cells by apoptosis. mRNA expression analysis confirmed that *Hmgcr* mRNA expression level in BAT of BAT KO mice was only 60.9% of that in BAT of Ctrl mice (Figure 7G); however, there was no significant difference in *Ucp1* mRNA expression levels (Figure 7H). In the cold tolerance test, cold exposure at 4°C decreased the rectal temperature of both genotypes, whereas Ctrl mice maintained the rectal temperature even under prolonged cold exposure. The rectal temperature of BAT KO mice gradually decreased and showed a significant decrease compared to that of Ctrl mice after 3 h of cold exposure (Figure 7I; Ctrl −3.5°C ± 0.15 vs. BAT KO −8.2°C ± 0.74, p = 0.0001). Infrared thermal images showed that dorsal surface temperatures were drastically reduced in BAT KO mice after cold exposure (Figure 7J). We also examined β_3-adrenergic receptor agonist CL316,243 (CL)-induced BAT thermogenesis. As shown in Figure 7K, administration of CL quickly increased the rectal temperature of Ctrl mice but not that of BAT KO mice. To investigate the role of the MVA pathway in BAT in adult mice, we generated tamoxifen-inducible adipocyte-specific *Hmgcr* KO (*Hmgcr*$^{flox/flox}$; *Adipoq-Cre*ER^{T2}; aiKO) mice. Twenty days after KO induction, we found a loss of lipid-containing adipocytes and the presence of apoptotic cells in the BAT of tamoxifen-treated aiKO mice (Figures 7L and 7M). As statin use has been reported to increase the risk of diabetes,[46] we investigated the effects of prolonged statin treatment on BAT and circular metabolic parameters in an

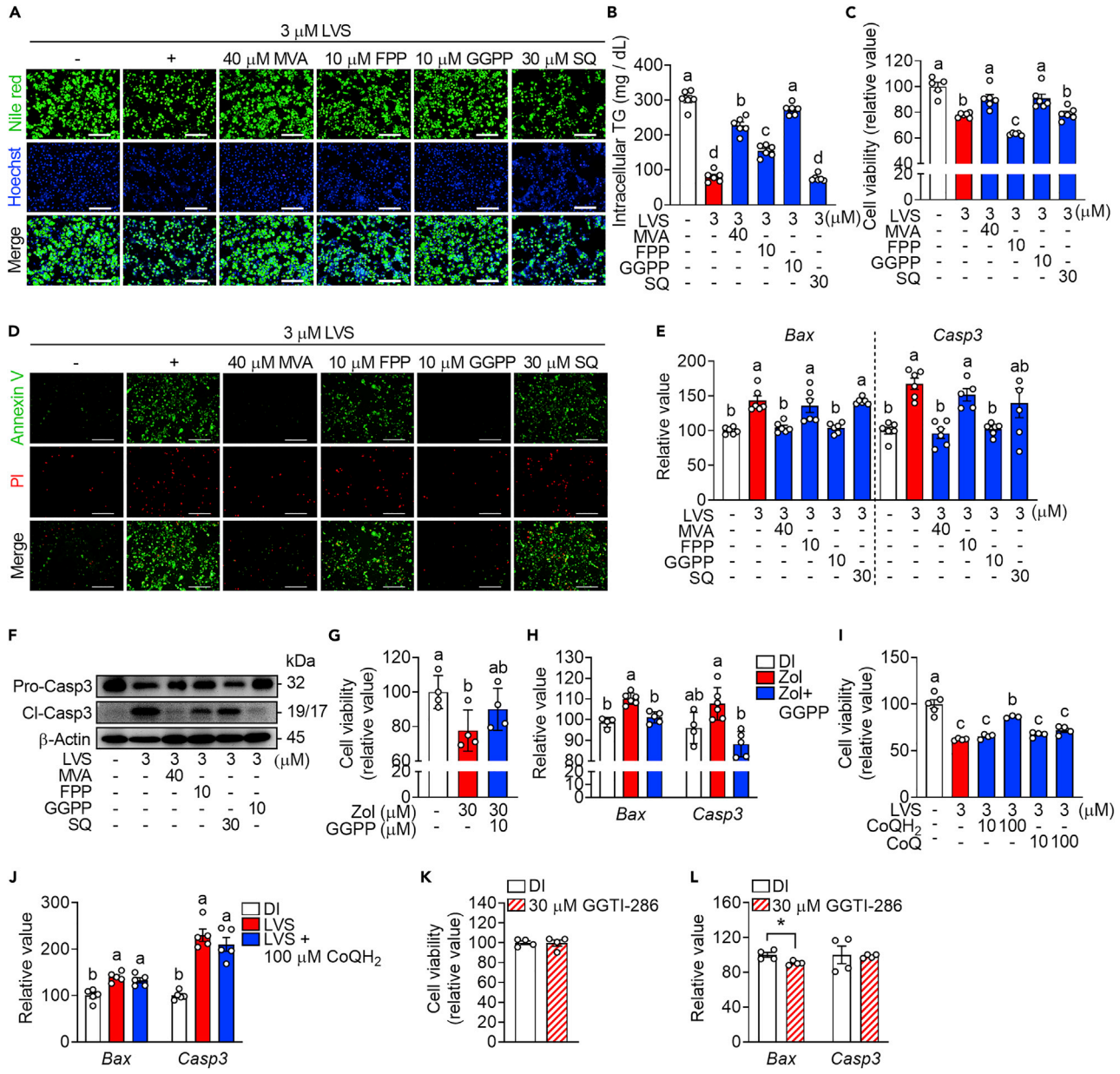

Figure 6. GGPP recovers LVS-induced cell apoptosis in mature brown adipocytes

(A) Representative microscopic view of DI- or LVS-treated HB2 cells with or without MVA, FPP, GGPP, or SQ treatment (days 4–8) after staining with Nile red (top) and Hoechst (middle) on day 8. Scale bars, 200 μm.

(B and C) Quantitative results of accumulated triglycerides (B; n = 6) and MTS assay (C; n = 5–6) in DI- or LVS-treated HB2 cells with or without MVA, FPP, GGPP, or SQ treatment (days 4–8) on day 8.

(D) Representative microscopic view of DI- or LVS-treated HB2 cells with or without MVA, FPP, GGPP, or SQ treatment (days 4–8) after staining with Annexin V (top) and propidium iodide (PI; middle) on day 8. Scale bars, 200 μm.

(E) Relative mRNA levels in DI- or LVS-treated HB2 cells with or without MVA, FPP, GGPP, or SQ treatment (days 4–8) on day 8 (n = 5–6).

(F) Representative immunoblots of pro-caspase 3 (Pro-Casp3) and cleaved caspase 3 (Cl-Casp3) in DI- or LVS-treated HB2 cells with or without MVA, FPP, SQ, or GGPP treatment (days 4–8) on day 8. β-Actin was used as a loading control.

(G and H) Results of MTS assay (G; n = 4) and relative mRNA levels (H; n = 4–6) in DI- or Zol-treated HB2 cells with or without GGPP (days 4–8) on day 8.

(I) MTS assay results of DI- or LVS-treated HB2 cells with or without $CoQH_2$ or CoQ treatment (days 4–8) on day 8 (n = 3–5).

Figure 6. *Continued*

(J) Relative mRNA levels in DI- or LVS-treated HB2 cells with or without $CoQH_2$ treatment (days 4–8) on day 8 (n = 5).

(K and L) Results of MTS assay (K; n = 4) and relative mRNA levels (L; n = 4) in DI- or GGTI-286-treated (days 4–8) HB2 cells on day 8. Data are shown as the mean ± SEM. *p < 0.05, unpaired two-tailed Student's *t* test for (L). Groups with different letters are significantly different (p < 0.05) as determined by one-way ANOVA with Tukey's HSD post-hoc analysis for (B), (C), (E), and (G–J). See also Figure S6.

obese diabetic mouse model (KK-A^y mouse[47]). Plasma total cholesterol levels were significantly decreased after 52 days of ATR treatment (Figure 7N; Veh 145.9 ± 7.1 vs. ATR 120.9 ± 5.8, p = 0.0216). Although BAT weight was not affected by ATR treatment (Figure S7A), morphologically altered areas, in which typical lipid-laden brown adipocytes did not exist, were observed in the BAT of KK-A^y mice treated with ATR (Figure 7O). Immunohistochemical analysis revealed abnormally aggregated perilipin (lipid-droplet-associated protein) and many apoptotic cells accumulated in these areas (Figure 7P). Moreover, although plasma triglyceride levels did not change (Figure S7B), plasma glucose levels were significantly increased by ATR treatment (Figure 7Q; Veh 174.6 ± 10.0 vs. ATR 254.4 ± 23.5, p = 0.0177), suggesting that ATR-induced apoptosis in BAT possibly contributes to hyperglycemia in KK-A^y mice. These findings clearly show that the MVA pathway in mature brown adipocytes is indispensable for maintaining BAT mass and function.

DISCUSSION

Increasing BAT thermogenesis, which can be achieved by enhancing BAT activity and mass, could be a promising strategy for treating obesity and obesity-induced T2D. In the present study, we demonstrated that MVA pathway–generated GGPP plays an indispensable role in retaining the thermogenic capacity of BAT by regulating BAT mass through controlling both brown adipogenesis and apoptosis of brown adipocytes. Notably, we demonstrated that distinct regulatory mechanisms govern brown adipogenesis and brown adipocyte survival via the MVA pathway; the former is partially dependent on geranylgeranylation (Figure 3), and the latter is independent of geranylgeranylation (Figure 6), respectively. Recently, Balaz et al.[18] reported that HMG-CoA synthase 2 is important for adipocyte browning. The authors showed that the MVA pathway–produced GGPP is essential for adipocyte browning by regulating geranylgeranylation-dependent yes-associated protein (YAP) / transcriptional coactivator with PDZ-binding motif (TAZ) signaling. Importantly, our findings, as well as those of the previous report, could highlight molecular mechanisms underlying a strong negative correlation between statin use and BAT prevalence.[10] Altogether, besides adipocyte browning, our findings demonstrate that GGPP also plays important roles in brown adipogenesis and brown adipocyte survival.

Hmgcr expression is regulated by SREBPs, which are transcription factors involved in the expression of key enzymes required for cholesterol, fatty acid, and triglyceride synthesis.[48] SREBP1/2 expression was upregulated in maternal cold-exposed fetal BAT.[49] Moreover, BAT-specific depletion of SREBP prevented the maintenance of body temperature under chronic cold exposure in mice.[50] These results suggest that the transcriptional activity of SREBPs in BAT is tightly regulated to maintain BAT function. In the present study, we showed that *Hmgcr* expression levels were altered in cold-innervated BAT and β-adrenergic receptor-activated cultured brown adipocytes, and these changes in expression levels were highly correlated with *Ucp1* expression levels (Figure 1). Therefore, SREBPs are candidate transcription factors that regulate the MVA pathway by modulating *Hmgcr* expression in the brown adipocytes.

During early adipocyte differentiation, growth-arrested preadipocytes re-enter the cell cycle, followed by transient mitosis, known as MCE, and subsequently express genes that produce adipocyte-specific phenotypes.[19,20] Forty-eight hours after the induction of differentiation, the DNA content of HB2 brown preadipocytes increased by more than 2-fold; however, the increase in DNA content was suppressed by LVS treatment (Figure 3F). GGPP supplementation completely recovered LVS-induced suppression of MCE (Figure 3F), suggesting that the MVA pathway plays an essential role in MCE during brown adipogenesis via the production of GGPP. MVA-mediated GGPP production appears to be important for substrate supply, at least partially for protein geranylgeranylation during MCE. Protein geranylgeranylation is especially important for anchoring small GTPases to the plasma membrane for their respective activation. Thus, inactivation of these small GTPases may be involved in inadequate MCE during brown adipogenesis. Geranylgeranylation of small G proteins is important for the proliferation of various cell types.[51–53] Our results, as well as those of several previous reports, suggest that GGPP is an important substrate for protein geranylgeranylation, which is essential for adequate MCE during brown adipocyte differentiation.

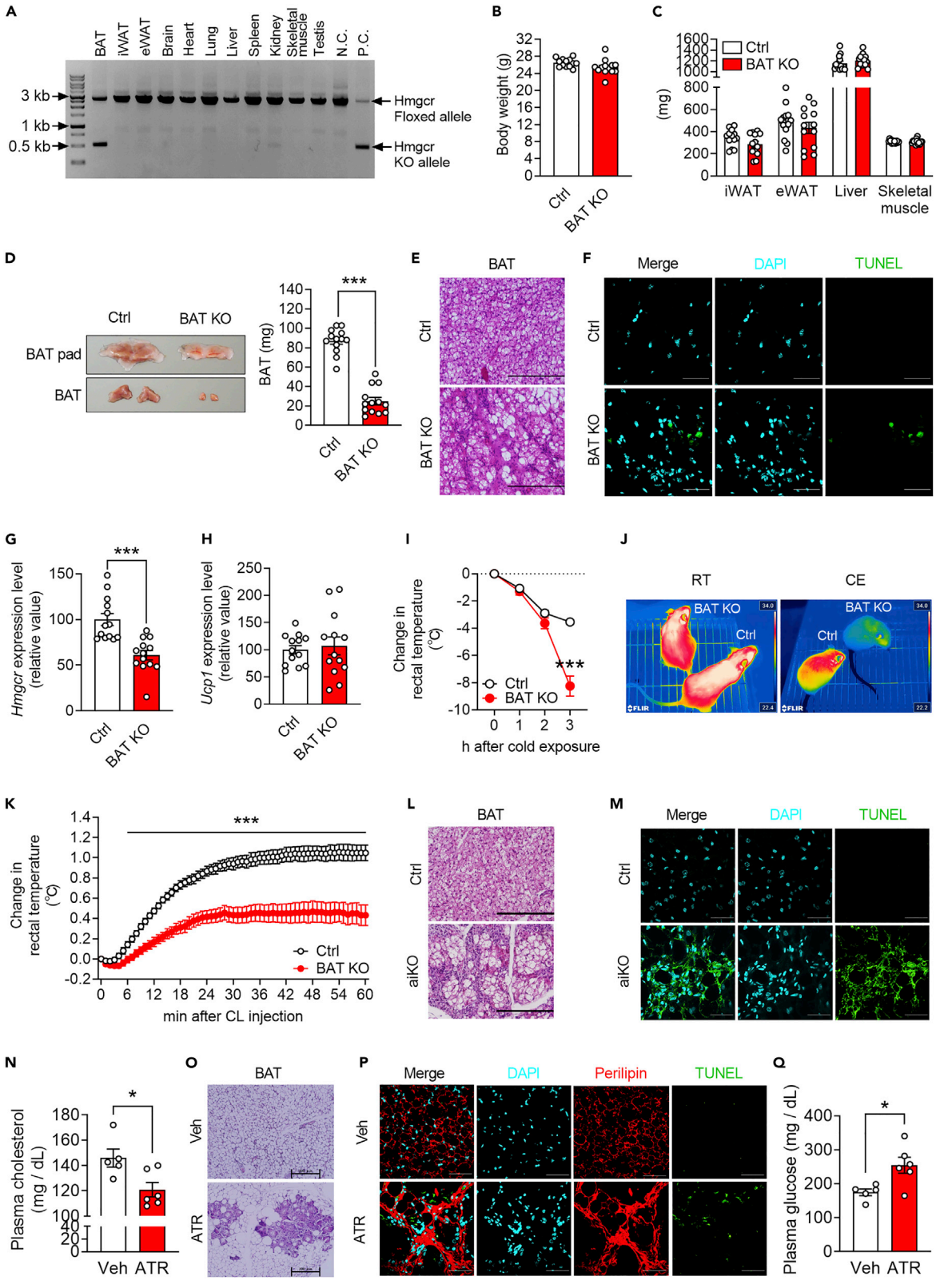
A
BAT
iWAT
eWAT
Brain
Heart
Lung
Liver
Spleen
Kidney
Skeletal muscle
Testis
N.C.
P.C.
3 kb
1 kb
0.5 kb
Hmgcr Floxed allele
Hmgcr KO allele
B
Body weight (g)
Ctrl
BAT KO
C
Ctrl
BAT KO
(mg)
iWAT
eWAT
Liver
Skeletal muscle
D
Ctrl
BAT KO
BAT pad
BAT
BAT (mg)
***
E
BAT
Ctrl
BAT KO
F
Merge
DAPI
TUNEL
G
Hmgcr expression level (relative value)
***
H
Ucp1 expression level (relative value)
I
Change in rectal temperature (°C)
Ctrl
BAT KO
***
h after cold exposure
J
RT
CE
BAT KO
Ctrl
K
Change in rectal temperature (°C)
***
min after CL injection
L
BAT
aiKO
M
Merge
DAPI
TUNEL
N
Plasma cholesterol (mg / dL)
*
Veh
ATR
O
BAT
P
Merge
DAPI
Perilipin
TUNEL
Q
Plasma glucose (mg / dL)
*

Figure 7. Brown adipocyte-specific *Hmgcr* knockout mice exhibit BAT atrophy and impaired thermoregulation

(A) Representative image from genotyping of BAT KO mice (n = 3). Top row, *Hmgcr*-floxed alleles (2757 bp); bottom row, *Hmgcr* knockout alleles (519 bp); N.C., negative control; P.C., positive control.

(B) Body weight of 14- to 15-week-old male Ctrl and BAT KO mice (n = 13).

(C) Weight of inguinal white adipose tissue (iWAT), epididymal white adipose tissue (eWAT), liver, and skeletal muscle (gastrocnemius + soleus) of the aforementioned mice (n = 13).

(D) Representative images (left) and weight of BAT (right; n = 13) from the aforementioned mice.

(E) Representative images of H&E-stained BAT section from 19-week-old male Ctrl and BAT KO mice. Scale bars, 200 μm.

(F) Representative immunofluorescence images of BAT isolated from 19-week-old male Ctrl and BAT KO mice. Scale bars, 30 μm.

(G and H) Relative mRNA levels of *Hmgcr* (G) and *Ucp1* (H) of BAT from 14- to 15-week-old male Ctrl and BAT KO mice (n = 13).

(I) Rectal temperature of 11- to 12-week-old male Ctrl and BAT KO mice exposed to cold at 4°C (n = 10–13).

(J) Infrared thermal images of 11- to 12-week-old male Ctrl and BAT KO mice before and after cold exposure at 6°C for 3 h. RT, room temperature exposed; CE, cold exposed.

(K) Rectal temperature of 11- to 12-week-old male Ctrl and BAT KO mice exposed to 1 mg/kg CL316,243 (n = 10–13).

(L) Representative images of H&E-stained BAT sections from 16-week-old male Ctrl and aiKO mice. Scale bars, 200 μm.

(M) Representative immunofluorescence images of BAT isolated from 16-week-old male Ctrl and aiKO mice. Scale bars, 30 μm.

(N) Plasma cholesterol levels in 6-h-fasted 11-week-old male KK-A^y mice treated with Veh or ATR (10 mg/kg/day) for 52 consecutive days (n = 5–6).

(O) Representative images of H&E-stained BAT sections from KK-A^y mice treated with Veh or ATR. Scale bars, 200 μm.

(P) Representative immunofluorescence images of BAT isolated from KK-A^y mice treated with Veh or ATR. Scale bars, 50 μm.

(Q) Plasma glucose levels in 6-h-fasted 11-week-old male KK-A^y mice treated with Veh or ATR (10 mg/kg/day) for 52 consecutive days (n = 5–6). Data are shown as the mean ± SEM. *p < 0.05, ***p < 0.001 by unpaired two-tailed Student's *t* test. See also Figure S7 and Table S1.

In this study, we demonstrated that statin treatment inhibits brown adipogenesis in HB2 cells. Consistently, we observed impaired BAT development in neonates exposed to LVS from E8.5 to E18.5, when differentiation of brown preadipocytes actively occurs.[40] These results suggest that MVA pathway–mediated regulation of brown adipocyte differentiation is important for BAT development *in vivo*. Previous studies have shown that Ewing sarcoma, bone-morphogenic protein 7, and homeobox A5 are critical regulators of brown adipogenesis in cultured cells, and its loss of function reduces BAT mass in mice.[54–57] These previous reports clearly indicate that the regulatory mechanisms of brown adipogenesis in cultured cells are closely related to BAT development *in vivo*. Therefore, MVA pathway–mediated regulation of brown adipocyte differentiation is thought to be important for BAT development *in vivo*. However, further studies are needed to investigate the effects of the MVA pathway on brown adipogenesis *in vivo*.

Statins inhibit multiple cellular functions of white adipocytes. For example, statin treatment triggers apoptosis in mature white adipocytes; however, this effect is reversed by GGPP treatment.[58] Similarly, we found that statin treatment induced apoptosis in mature brown adipocytes, which was possibly associated with the lack of downstream products from GGPP. Moreover, statin treatment impairs white adipogenesis by reducing the expression levels of C/EBPβ, C/EBPα, and PPARγ,[44,59,60] which is consistent with the findings of our study showing reduced adipocyte markers after LVS treatment in differentiating brown adipocytes. In particular, we observed a decrease in nuclear C/EBPβ expression in differentiating brown adipocytes upon LVS treatment. Importantly, C/EBPβ functions not only as a regulator of early adipogenesis[61] but also as a fate switch in thermogenic adipocytes.[62,63] Although most mechanisms underlying statin effects on brown adipocytes and white adipocytes may be similar, further investigation, especially regarding cellular fate, is needed to determine whether statins function as a molecular switch in determining thermogenic adipocyte development.

Although the differentiation of white adipocyte and brown adipocyte is controlled by a similar set of transcription factors, including C/EBPβ, their contribution to the adipocyte differentiation process may differ. The active form of C/EBPβ (LAP) serves as a critical regulator of brown adipogenesis by forming a transcriptional complex with PRDM16, a transcription factor that regulates thermogenic genes in brown adipocytes.[63] One known regulator of C/EBPβ function is RB, which is an important regulator of cell cycle processes and cellular differentiation.[64–66] In 3T3-L1 cells, RB hyperphosphorylation (inactive) induced by adipocyte differentiation stimuli has been implicated in the regulation of adipocyte differentiation via physical interactions with C/EBPβ and in the regulation of its transcriptional activity.[45] RB-deficient mouse embryonic fibroblasts differentiate into adipocytes with a gene expression pattern resembling that of brown adipocytes.[67] We demonstrated that LVS treatment suppressed the differentiation stimuli-induced inactivation of RB and the simultaneous nuclear localization of C/EBPβ in HB2 cells, which could be highly informative regarding the essential role of RB in the MVA pathway–mediated regulation of brown adipocyte differentiation.

Several studies using tissue-specific *Hmgcr* KO mice have shown that the MVA pathway is an important physiological regulator of cell survival by producing non-sterol isoprenoid intermediates in various cells.[15,58,68,69] However, the mechanism by which the MVA pathway affects mature brown adipocytes remains unclear. In this study, we showed that disruption of the MVA pathway causes programmed cell death owing to a lack of GGPP synthesis in mature brown adipocytes. Unlike LVS treatment, treatment with a GGTase I inhibitor did not induce apoptosis in brown adipocytes, suggesting the involvement of mechanisms independent of protein geranylgeranylation. The possible involvement of coenzyme Q_{10} deficiency in statin-induced cell death has been reported in several cell types, such as myotubes and hepatocytes.[70,71] However, in the present study, GGPP deficiency–induced apoptosis was not attributed to a coenzyme Q_{10} deficiency. Therefore, other metabolites derived from GGPP may be involved in statin-induced apoptosis in brown adipocytes. Liver X receptors (LXRs) were shown to regulate statin-induced cell death in 3T3-L1 cells.[72] LXRs suppress proliferation of various cancer cells. For example, Zhang et al.[73] showed that treatment with T0901317, a synthetic LXR agonist, suppresses the proliferation of melanoma cells by activating caspase 3, suggesting that LXRs play an important role in cell survival. Interestingly, GGPP has been reported to regulate the function of LXRs by acting as a direct antagonist.[74,75] These reports highlight the possibility that GGPP-mediated LXRs regulation may play an important role in *Hmgcr* deficiency–induced apoptosis in brown adipocytes.

Niemann et al.[76] reported that apoptotic brown adipocytes induce *de novo* brown adipogenesis in BAT through the action of inosine to maintain BAT mass. Although brown adipocyte apoptosis occurred in BAT (Figure 7F), BAT atrophy was observed (Figure 7D) in BAT KO mice, suggesting that the formation of new brown adipocytes in BAT KO mice is very limited. Niemann et al.[76] showed that extracellular inosine activates the mammalian target of rapamycin complex 1 (mTORC1) in brown adipocytes, suggesting that mTORC1 may be involved in inosine-induced brown adipogenesis. The importance of mTORC1 signaling in BAT development has been reported by several study groups. For example, mTORC1 inhibition by rapamycin or siRNA decreased the proliferation and differentiation of brown adipocytes.[77] Adipocyte-specific mTORC1 loss in mice completely blocked cold-induced BAT recruitment.[78] Importantly, statin treatment suppresses mTOR signaling,[79] suggesting that the MVA pathway regulates mTOR signaling. The small GTPase Rac1, a target of GGTase I, regulates mTORC1 activity.[80] In Figures 3P–3R, we demonstrated that treatment with a GGTase I inhibitor suppressed brown adipocyte differentiation, suggesting that GGPP depletion by statins might suppress the geranylgeranylated Rac1-mTORC1 axis. This pathway may be involved in the inosine-induced differentiation of brown adipocytes.

In conclusion, the MVA pathway appears to be critical for maintaining brown adipocyte function by regulating both differentiation and apoptosis of brown adipocytes. GGPP is a pivotal isoprenoid produced by the MVA pathway in both processes. Our results highlight the importance of the MVA pathway in brown adipocytes to identify mechanisms that can be employed to develop therapeutic approaches for lowering statin-induced side effects, such as T2D.

Limitations of the study

We demonstrated that LVS treatment to fetuses during the BAT developmental period impaired BAT formation in neonates, suggesting the pivotal role of MVA pathway in brown adipocyte differentiation. However, we cannot rule out the possibility that LVS-induced cell apoptosis of mature brown adipocytes also contributes to BAT atrophy in neonates. There is also a possibility that inhibition of MVA pathway by LVS affects the fate of potential progenitors for brown adipocytes *in vivo*. Further study is still needed to fully clarify the effects of the MVA pathway on brown adipogenesis *in vivo*. Another limitation is that we could not measure the actual cellular and tissue GGPP levels, so it is necessary to confirm the exact amount of GGPP required for normal BAT maintenance. We hopefully clarify these important limitations in our future studies.

STAR★METHODS

Detailed methods are provided in the online version of this paper and include the following:

- KEY RESOURCES TABLE
- RESOURCE AVAILABILITY
  - Lead contact
  - Materials availability
  - Data and code availability
- EXPERIMENTAL MODEL AND SUBJECT DETAILS

SUPPLEMENTAL INFORMATION

Supplemental information can be found online at https://doi.org/10.1016/j.isci.2023.106161.

ACKNOWLEDGMENTS

The authors sincerely thank Assoc. Prof. Taiho Kambe (Kyoto University, Japan) for helpful advice on the subcellular fractionation experiment. The authors are grateful to Prof. Yusaku Iwasaki (Kyoto Prefectural University, Japan) for technical advice on rectal temperature measurement of mice. The authors also thank Su-Ping Ng for improving the use of English, Rika Yoshii for secretarial support, and Masaomi Komori for technical support. This study was supported by JSPS KAKENHI: grant numbers JP19H02910, JP20K21755, and JP22H02287.

AUTHOR CONTRIBUTIONS

T.G. and Y.-S.Y. conceived and designed the experiments. J.K. designed the experiments and conducted most of the experiments and collected and analyzed data. Y.-S.Y. conducted animal experiments related to KK-A^y mice and collected and analyzed data. S.K. conducted *in vivo* fluorescence imaging for postnatal mice. S.M. assisted with animal experiments. Y.O.-O., K.K., and M.S. supported experiments using HB2 cells. H.M., Y.F., and N.I. supported animal experiments especially those using infrared thermography. Y.O.-O., H.T., W.N., R.Y., K.K., M.S., K.I., and T.K. provided expertise and feedback. J.K. and T.G. interpreted data and wrote the manuscript. T.G. was involved in project planning and supervision.

DECLARATION OF INTERESTS

The authors declare no competing interests.

Received: August 2, 2022
Revised: January 8, 2023
Accepted: February 3, 2023
Published: February 8, 2023

REFERENCES

1. Mokdad, A.H., Ford, E.S., Bowman, B.A., Dietz, W.H., Vinicor, F., Bales, V.S., and Marks, J.S. (2003). Prevalence of obesity, diabetes, and obesity-related health risk factors, 2001. JAMA *289*, 76–79. https://doi.org/10.1001/jama.289.1.76.

2. Steinberger, J., and Daniels, S.R. (2003). Obesity, insulin resistance, diabetes, and cardiovascular risk in children: an American Heart Association scientific statement from the atherosclerosis, hypertension, and obesity in the young committee (council on cardiovascular disease in the young) and the diabetes committee (council on nutrition, physical activity, and metabolism). Circulation *107*, 1448–1453. https://doi.org/10.1161/01.CIR.0000060923.07573.F2.

3. Bartelt, A., Bruns, O.T., Reimer, R., Hohenberg, H., Ittrich, H., Peldschus, K., Kaul, M.G., Tromsdorf, U.I., Weller, H., Waurisch, C., et al. (2011). Brown adipose tissue activity controls triglyceride clearance. Nat. Med. *17*, 200–205. https://doi.org/10.1038/nm.2297.

4. Chondronikola, M., Volpi, E., Børsheim, E., Porter, C., Saraf, M.K., Annamalai, P., Yfanti, C., Chao, T., Wong, D., Shinoda, K., et al. (2016). Brown adipose tissue activation is linked to distinct systemic effects on lipid metabolism in humans. Cell Metab. *23*,

1200–1206. https://doi.org/10.1016/j.cmet.2016.04.029.

5. Stanford, K.I., Middelbeek, R.J.W., Townsend, K.L., An, D., Nygaard, E.B., Hitchcox, K.M., Markan, K.R., Nakano, K., Hirshman, M.F., Tseng, Y.-H., and Goodyear, L.J. (2013). Brown adipose tissue regulates glucose homeostasis and insulin sensitivity. J. Clin. Invest. *123*, 215–223. https://doi.org/10.1172/JCI62308.

6. Yoneshiro, T., Wang, Q., Tajima, K., Matsushita, M., Maki, H., Igarashi, K., Dai, Z., White, P.J., McGarrah, R.W., Ilkayeva, O.R., et al. (2019). BCAA catabolism in brown fat controls energy homeostasis through SLC25A44. Nature *572*, 614–619. https://doi.org/10.1038/s41586-019-1503-x.

7. Carpentier, A.C., Blondin, D.P., Virtanen, K.A., Richard, D., Haman, F., and Turcotte, É.E. (2018). Brown adipose tissue energy metabolism in humans. Front. Endocrinol. *9*, 447. https://doi.org/10.3389/fendo.2018.00447.

8. Saito, M., Okamatsu-Ogura, Y., Matsushita, M., Watanabe, K., Yoneshiro, T., Nio-Kobayashi, J., Iwanaga, T., Miyagawa, M., Kameya, T., Nakada, K., et al. (2009). High incidence of metabolically active brown adipose tissue in healthy adult humans: effects of cold exposure and adiposity. Diabetes *58*, 1526–1531. https://doi.org/10.2337/db09-0530.

9. Vijgen, G.H.E.J., Bouvy, N.D., Teule, G.J.J., Brans, B., Schrauwen, P., and van Marken Lichtenbelt, W.D. (2011). Brown adipose tissue in morbidly obese subjects. PLoS One *6*, e17247. https://doi.org/10.1371/journal.pone.0017247.

10. Becher, T., Palanisamy, S., Kramer, D.J., Eljalby, M., Marx, S.J., Wibmer, A.G., Butler, S.D., Jiang, C.S., Vaughan, R., Schöder, H., et al. (2021). Brown adipose tissue is associated with cardiometabolic health. Nat. Med. *27*, 58–65. https://doi.org/10.1038/s41591-020-1126-7.

11. Goldstein, J.L., and Brown, M.S. (1990). Regulation of the mevalonate pathway. Nature *343*, 425–430. https://doi.org/10.1038/343425a0.

12. Casey, P.J. (1992). Biochemistry of protein prenylation. J. Lipid Res. *33*, 1731–1740. https://doi.org/10.1016/S0022-2275(20)41331-8.

13. Oesterle, A., Laufs, U., and Liao, J.K. (2017). Pleiotropic effects of statins on the cardiovascular system. Circ. Res. *120*, 229–243. https://doi.org/10.1161/CIRCRESAHA.116.308537.

14. Newman, C.B., Preiss, D., Tobert, J.A., Jacobson, T.A., Page, R.L., Goldstein, L.B., Chin, C., Tannock, L.R., Miller, M., Raghuveer, G., et al. (2019). Statin safety and associated adverse events: a scientific statement from the American Heart Association. Arterioscler. Thromb. Vasc. Biol. *39*, E38–E81. https://doi.org/10.1161/ATV.0000000000000073.

15. de Giorgi, M., Jarrett, K.E., Burton, J.C., Doerfler, A.M., Hurley, A., Li, A., Hsu, R.H., Furgurson, M., Patel, K.R., Han, J., et al. (2020). Depletion of essential isoprenoids and ER stress induction following acute liver-specific deletion of HMG-CoA reductase. J. Lipid Res. *61*, 1675–1686. https://doi.org/10.1194/jlr.RA120001006.

16. Nagashima, S., Yagyu, H., Ohashi, K., Tazoe, F., Takahashi, M., Ohshiro, T., Bayasgalan, T., Okada, K., Sekiya, M., Osuga, J.-i., and Ishibashi, S. (2012). Liver-specific deletion of 3-hydroxy-3-methylglutaryl coenzyme A reductase causes hepatic steatosis and death. Arterioscler. Thromb. Vasc. Biol. *32*, 1824–1831. https://doi.org/10.1161/ATVBAHA.111.240754.

17. Osaki, Y., Nakagawa, Y., Miyahara, S., Iwasaki, H., Ishii, A., Matsuzaka, T., Kobayashi, K., Yatoh, S., Takahashi, A., Yahagi, N., et al. (2015). Skeletal muscle-specific HMG-CoA reductase knockout mice exhibit rhabdomyolysis: a model for statin-induced myopathy. Biochem. Biophys. Res. Commun. *466*, 536–540. https://doi.org/10.1016/j.bbrc.2015.09.065.

18. Balaz, M., Becker, A.S., Balazova, L., Straub, L., Müller, J., Gashi, G., Maushart, C.I., Sun, W., Dong, H., Moser, C., et al. (2019). Inhibition of mevalonate pathway prevents adipocyte browning in mice and men by affecting protein prenylation. Cell Metab. *29*, 901–916.e8. https://doi.org/10.1016/j.cmet.2018.11.017.

19. Rosen, E.D., Walkey, C.J., Puigserver, P., and Spiegelman, B.M. (2000). Transcriptional regulation of adipogenesis. Genes Dev. *14*, 1293–1307. https://doi.org/10.1101/gad.14.11.1293.

20. Tang, Q.-Q., Otto, T.C., and Lane, M.D. (2003). Mitotic clonal expansion: a synchronous process required for adipogenesis. Proc. Natl. Acad. Sci. USA *100*, 44–49. https://doi.org/10.1073/pnas.0137044100.

21. Hishida, T., Nishizuka, M., Osada, S., and Imagawa, M. (2009). The role of C/EBPδ in the early stages of adipogenesis. Biochimie *91*, 654–657. https://doi.org/10.1016/j.biochi.2009.02.002.

22. Tang, Q.-Q., Otto, T.C., and Lane, M.D. (2003). CCAAT/enhancer-binding protein β is required for mitotic clonal expansion during adipogenesis. Proc. Natl. Acad. Sci. USA *100*, 850–855. https://doi.org/10.1073/pnas.0337434100.

23. Clarke, S.L., Robinson, C.E., and Gimble, J.M. (1997). CAAT/enhancer binding proteins directly modulate transcription from the peroxisome proliferator-activated receptor γ2 promoter. Biochem. Biophys. Res. Commun. *240*, 99–103. https://doi.org/10.1006/bbrc.1997.7627.

24. Tang, Q.-Q., Jiang, M.-S., and Lane, M.D. (1999). Repressive effect of Sp1 on the C/EBPα gene promoter: role in adipocyte differentiation. Mol. Cell Biol. *19*, 4855–4865. https://doi.org/10.1128/MCB.19.7.4855.

25. Elmore, S. (2007). Apoptosis: a review of programmed cell death. Toxicol. Pathol. *35*, 495–516. https://doi.org/10.1080/01926230701320337.

26. Spalding, K.L., Arner, E., Westermark, P.O., Bernard, S., Buchholz, B.A., Bergmann, O., Blomqvist, L., Hoffstedt, J., Näslund, E., Britton, T., et al. (2008). Dynamics of fat cell turnover in humans. Nature *453*, 783–787. https://doi.org/10.1038/nature06902.

27. Kim, S.M., Lun, M., Wang, M., Senyo, S.E., Guillermier, C., Patwari, P., and Steinhauser, M.L. (2014). Loss of white adipose hyperplastic potential is associated with enhanced susceptibility to insulin resistance. Cell Metab. *20*, 1049–1058. https://doi.org/10.1016/j.cmet.2014.10.010.

28. Yamauchi, T., Kamon, J., Waki, H., Murakami, K., Motojima, K., Komeda, K., Ide, T., Kubota, N., Terauchi, Y., Tobe, K., et al. (2001). The mechanisms by which both heterozygous peroxisome proliferator-activated receptor γ (PPARγ) deficiency and PPARγ agonist improve insulin resistance. J. Biol. Chem. *276*, 41245–41254. https://doi.org/10.1074/jbc.M103241200.

29. He, W., Barak, Y., Hevener, A., Olson, P., Liao, D., Le, J., Nelson, M., Ong, E., Olefsky, J.M., and Evans, R.M. (2003). Adipose-specific peroxisome proliferator-activated receptor γ knockout causes insulin resistance in fat and liver but not in muscle. Proc. Natl. Acad. Sci. USA *100*, 15712–15717. https://doi.org/10.1073/pnas.253682810.

30. Lynes, M.D., Schulz, T.J., Pan, A.J., and Tseng, Y.H. (2015). Disruption of insulin signaling in Myf5-expressing progenitors leads to marked paucity of brown fat but normal muscle development. Endocrinology *156*, 1637–1647. https://doi.org/10.1210/en.2014-1773.

31. Zhao, J., Yang, Q., Zhang, L., Liang, X., Sun, X., Wang, B., Chen, Y., Zhu, M., and Du, M. (2017). AMPKα1 deficiency suppresses brown adipogenesis in favor of fibrogenesis during brown adipose tissue development. Biochem. Biophys. Res. Commun. *491*, 508–514. https://doi.org/10.1016/j.bbrc.2017.06.149.

32. Guerra, C., Navarro, P., Valverde, A.M., Arribas, M., Brüning, J., Kozak, L.P., Kahn, C.R., and Benito, M. (2001). Brown adipose tissue–specific insulin receptor knockout shows diabetic phenotype without insulin resistance. J. Clin. Invest. *108*, 1205–1213. https://doi.org/10.1172/JCI13103.

33. Xiong, W., Zhao, X., Villacorta, L., Rom, O., Garcia-Barrio, M.T., Guo, Y., Fan, Y., Zhu, T., Zhang, J., Zeng, R., et al. (2018). Brown adipocyte-specific PPARγ (peroxisome proliferator-activated receptor γ) deletion impairs perivascular adipose tissue development and enhances atherosclerosis in mice. Arterioscler. Thromb. Vasc. Biol. *38*, 1738–1747. https://doi.org/10.1161/ATVBAHA.118.311367.

34. Yue, F., Cheng, Y., Breschi, A., Vierstra, J., Wu, W., Ryba, T., Sandstrom, R., Ma, Z., Davis, C., Pope, B.D., et al. (2014). A comparative encyclopedia of DNA elements in the mouse genome. Nature *515*, 355–364. https://doi.org/10.1038/nature13992.

35. Hooff, G.P., Peters, I., Wood, W.G., Müller, W.E., and Eckert, G.P. (2010). Modulation of cholesterol, farnesylpyrophosphate, and geranylgeranylpyrophosphate in neuroblastoma SH-SY5Y-APP695 cells: impact on amyloid beta-protein production. Mol. Neurobiol. *41*, 341–350. https://doi.org/10.1007/s12035-010-8117-5.

36. Tong, H., Holstein, S.A., and Hohl, R.J. (2005). Simultaneous determination of farnesyl and geranylgeranyl pyrophosphate levels in cultured cells. Anal. Biochem. *336*, 51–59. https://doi.org/10.1016/j.ab.2004.09.024.

37. No, J.H., de Macedo Dossin, F., Zhang, Y., Liu, Y.-L., Zhu, W., Feng, X., Yoo, J.A., Lee, E., Wang, K., Hui, R., et al. (2012). Lipophilic analogs of zoledronate and risedronate inhibit Plasmodium geranylgeranyl diphosphate synthase (GGPPS) and exhibit potent antimalarial activity. Proc. Natl. Acad. Sci. USA *109*, 4058–4063. https://doi.org/10.1073/pnas.1118215109.

38. Anderson, C.M., Kazantzis, M., Wang, J., Venkatraman, S., Goncalves, R.L.S., Quinlan, C.L., Ng, R., Jastroch, M., Benjamin, D.I., Nie, B., et al. (2015). Dependence of brown adipose tissue function on CD36-mediated coenzyme Q uptake. Cell Rep. *10*, 505–515. https://doi.org/10.1016/j.celrep.2014.12.048.

39. Zhang, F.L., and Casey, P.J. (1996). Influence of metal ions on substrate binding and catalytic activity of mammalian protein geranylgeranyltransferase type-I. Biochem. J. *320*, 925–932. https://doi.org/10.1042/bj3200925.

40. Song, A., Dai, W., Jang, M.J., Medrano, L., Li, Z., Zhao, H., Shao, M., Tan, J., Li, A., Ning, T., et al. (2020). Low-and high-thermogenic brown adipocyte subpopulations coexist in murine adipose tissue. J. Clin. Invest. *130*, 247–257. https://doi.org/10.1172/JCI129167.

41. Kawarasaki, S., Kuwata, H., Sawazaki, H., Sakamoto, T., Nitta, T., Kim, C.S., Jheng, H.-F., Takahashi, H., Nomura, W., Ara, T., et al. (2019). A new mouse model for noninvasive fluorescence-based monitoring of mitochondrial UCP1 expression. FEBS Lett. *593*, 1201–1212. https://doi.org/10.1002/1873-3468.13430.

42. Fukano, K., Okamatsu-Ogura, Y., Tsubota, A., Nio-Kobayashi, J., and Kimura, K. (2016). Cold exposure induces proliferation of mature brown adipocyte in a β3-adrenergic receptor-mediated pathway. PLoS One *11*, e0166579. https://doi.org/10.1371/journal.pone.0166579.

43. Shin, S., Pang, Y., Park, J., Liu, L., Lukas, B.E., Kim, S.H., Kim, K.-W., Xu, P., Berry, D.C., and Jiang, Y. (2020). Dynamic control of adipose tissue development and adult tissue homeostasis by platelet-derived growth factor receptor alpha. Elife *9*, e56189. https://doi.org/10.7554/eLife.56189.

44. Mäuser, W., Perwitz, N., Meier, B., Fasshauer, M., and Klein, J. (2007). Direct adipotropic actions of atorvastatin: differentiation state-dependent induction of apoptosis, modulation of endocrine function, and inhibition of glucose uptake. Eur. J. Pharmacol. *564*, 37–46. https://doi.org/10.1016/j.ejphar.2007.02.024.

45. Cole, K.A., Harmon, A.W., Harp, J.B., and Patel, Y.M. (2004). Rb regulates C/EBPβ-DNA-binding activity during 3T3-L1 adipogenesis. Am. J. Physiol. Cell Physiol. *286*, C349–C354. https://doi.org/10.1152/ajpcell.00255.2003.

46. Zaharan, N.L., Williams, D., and Bennett, K. (2013). Statins and risk of treated incident diabetes in a primary care population. Br. J. Clin. Pharmacol. *75*, 1118–1124. https://doi.org/10.1111/j.1365-2125.2012.04403.x.

47. Nishimura, M. (1969). Breeding of mice strains for diabetes mellitus. Exp. Anim. *18*, 147–157. https://doi.org/10.1538/expanim1957.18.4_147.

48. Eberlé, D., Hegarty, B., Bossard, P., Ferré, P., and Foufelle, F. (2004). SREBP transcription factors: master regulators of lipid homeostasis. Biochimie *86*, 839–848. https://doi.org/10.1016/j.biochi.2004.09.018.

49. Ghosh, S., Park, C.H., Lee, J., Lee, N., Zhang, R., Huesing, C., Reijnders, D., Sones, J., Münzberg, H., Redman, L., and Chang, J.S. (2021). Maternal cold exposure induces distinct transcriptome changes in the placenta and fetal brown adipose tissue in mice. BMC Genomics *22*, 500. https://doi.org/10.1186/s12864-021-07825-6.

50. Adlanmerini, M., Carpenter, B.J., Remsberg, J.R., Aubert, Y., Peed, L.C., Richter, H.J., and Lazar, M.A. (2019). Circadian lipid synthesis in brown fat maintains murine body temperature during chronic cold. Proc. Natl. Acad. Sci. USA *116*, 18691–18699. https://doi.org/10.1073/pnas.1909883116.

51. Chong, D., Chen, Z., Guan, S., Zhang, T., Xu, N., Zhao, Y., and Li, C. (2021). Geranylgeranyl pyrophosphate-mediated protein geranylgeranylation regulates endothelial cell proliferation and apoptosis during vasculogenesis in mouse embryo. J. Genet. Genomics *48*, 300–311. https://doi.org/10.1016/j.jgg.2021.03.009.

52. Khwaja, A., Sharpe, C.C., Noor, M., and Hendry, B.M. (2006). The role of geranylgeranylated proteins in human mesangial cell proliferation. Kidney Int. *70*, 1296–1304. https://doi.org/10.1038/sj.ki.5001713.

53. Philips, M.R., and Cox, A.D. (2007). Geranylgeranyltransferase I as a target for anti-cancer drugs. J. Clin. Invest. *117*, 1223–1225. https://doi.org/10.1172/JCI32108.

54. Cao, W., Huang, H., Xia, T., Liu, C., Muhammad, S., and Sun, C. (2018). Homeobox a5 promotes white adipose tissue browning through inhibition of the tenascin C/toll-like receptor 4/nuclear factor kappa B inflammatory signaling in mice. Front. Immunol. *9*, 647. https://doi.org/10.3389/fimmu.2018.006.

55. Holzman, M.A., Ryckman, A., Finkelstein, T.M., Landry-Truchon, K., Schindler, K.A., Bergmann, J.M., Jeannotte, L., and Mansfield, J.H. (2021). HOXA5 participates in Brown adipose tissue and epaxial skeletal muscle patterning and in Brown adipocyte differentiation. Front. Cell Dev. Biol. *9*, 632303. https://doi.org/10.3389/fcell.2021.632303.

56. Park, J.H., Kang, H.J., Kang, S.I., Lee, J.E., Hur, J., Ge, K., Mueller, E., Li, H., Lee, B.-C., and Lee, S.B. (2013). A multifunctional protein, EWS, is essential for early brown fat lineage determination. Dev. Cell *26*, 393–404. https://doi.org/10.1016/j.devcel.2013.07.002.

57. Tseng, Y.-H., Kokkotou, E., Schulz, T.J., Huang, T.L., Winnay, J.N., Taniguchi, C.M., Tran, T.T., Suzuki, R., Espinoza, D.O., Yamamoto, Y., et al. (2008). New role of bone morphogenetic protein 7 in brown adipogenesis and energy expenditure. Nature *454*, 1000–1004. https://doi.org/10.1038/nature07221.

58. Yeh, Y.-S., Jheng, H.-F., Iwase, M., Kim, M., Mohri, S., Kwon, J., Kawarasaki, S., Li, Y., Takahashi, H., Ara, T., et al. (2018). The mevalonate pathway is indispensable for adipocyte survival. iScience *9*, 175–191. https://doi.org/10.1016/j.isci.2018.10.019.

59. Li, X., Cui, Q., Kao, C., Wang, G.J., and Balian, G. (2003). Lovastatin inhibits adipogenic and stimulates osteogenic differentiation by suppressing PPARγ2 and increasing Cbfa1/Runx2 expression in bone marrow mesenchymal cell cultures. Bone *33*, 652–659. https://doi.org/10.1016/S8756-3282(03)00239-4.

60. Nakata, M., Nagasaka, S., Kusaka, I., Matsuoka, H., Ishibashi, S., and Yada, T. (2006). Effects of statins on the adipocyte maturation and expression of glucose transporter 4 (SLC2A4): implications in glycaemic control. Diabetologia *49*, 1881–1892. https://doi.org/10.1007/s00125-006-0269-5.

61. Guo, L., Li, X., and Tang, Q.Q. (2015). Transcriptional regulation of adipocyte differentiation: a central role for CCAAT/enhancer-binding protein (C/EBP) β. J. Biol. Chem. *290*, 755–761. https://doi.org/10.1074/jbc.R114.619957.

62. Fukunaka, A., Fukada, T., Bhin, J., Suzuki, L., Tsuzuki, T., Takamine, Y., Bin, B.-H., Yoshihara, T., Ichinoseki-Sekine, N., Naito, H., et al. (2017). Zinc transporter ZIP13 suppresses beige adipocyte biogenesis and energy expenditure by regulating C/EBP-β expression. PLoS Genet. *13*, e1006950. https://doi.org/10.1371/journal.pgen.1006950.

63. Kajimura, S., Seale, P., Kubota, K., Lunsford, E., Frangioni, J.V., Gygi, S.P., and Spiegelman, B.M. (2009). Initiation of myoblast to brown fat switch by a PRDM16–C/EBP-β transcriptional complex. Nature *460*, 1154–1158. https://doi.org/10.1038/nature08262.

64. Charles, A., Tang, X., Crouch, E., Brody, J.S., and Xiao, Z.X. (2001). Retinoblastoma protein complexes with C/EBP proteins and activates C/EBP-mediated transcription. J. Cell. Biochem. *83*, 414–425. https://doi.org/10.1002/jcb.1239.

65. Chen, P.L., Riley, D.J., Chen, Y., and Lee, W.H. (1996). Retinoblastoma protein positively regulates terminal adipocyte differentiation through direct interaction with C/EBPs. Genes Dev. *10*, 2794–2804. https://doi.org/10.1101/gad.10.21.2794.

66. Khidr, L., and Chen, P.L. (2006). RB, the conductor that orchestrates life, death and differentiation. Oncogene *25*, 5210–5219. https://doi.org/10.1038/sj.onc.1209612.

67. Hansen, J.B., Jørgensen, C., Petersen, R.K., Hallenborg, P., de Matteis, R., Bøye, H.A., Petrovic, N., Enerbäck, S., Nedergaard, J., Cinti, S., et al. (2004). Retinoblastoma protein functions as a molecular switch determining white versus brown adipocyte differentiation. Proc. Natl. Acad. Sci. USA *101*, 4112–4117. https://doi.org/10.1073/pnas.0301964101.

68. Lacher, S.M., Bruttger, J., Kalt, B., Berthelet, J., Rajalingam, K., Wörtge, S., and Waisman, A. (2017). HMG-CoA reductase promotes protein prenylation and therefore is indispensible for T-cell survival. Cell Death Dis. *8*, e2824. https://doi.org/10.1038/cddis.2017.221.

69. Ohashi, K., Osuga, J.I., Tozawa, R., Kitamine, T., Yagyu, H., Sekiya, M., Tomita, S., Okazaki, H., Tamura, Y., Yahagi, N., et al. (2003). Early embryonic lethality caused by targeted disruption of the 3-hydroxy-3-methylglutaryl-CoA reductase gene. J. Biol. Chem. *278*, 42936–42941. https://doi.org/10.1074/jbc.M307228200.

70. Moschetti, A., Dagda, R.K., and Ryan, R.O. (2021). Coenzyme Q nanodisks counteract the effect of statins on C2C12 myotubes. Nanomedicine. *37*, 102439. https://doi.org/10.1016/j.nano.2021.102439.

71. Tavintharan, S., Ong, C.N., Jeyaseelan, K., Sivakumar, M., Lim, S.C., and Sum, C.F. (2007). Reduced mitochondrial coenzyme Q10 levels in HepG2 cells treated with high-dose simvastatin: a possible role in statin-induced hepatotoxicity? Toxicol. Appl. Pharmacol. *223*, 173–179. https://doi.org/10.1016/j.taap.2007.05.013.

72. Madsen, L., Petersen, R.K., Steffensen, K.R., Pedersen, L.M., Hallenborg, P., Ma, T., Frøyland, L., Døskeland, S.O., Gustafsson, J.Å., and Kristiansen, K. (2008). Activation of liver X receptors prevents statin-induced death of 3T3-L1 preadipocytes. J. Biol. Chem. *283*, 22723–22736. https://doi.org/10.1074/jbc.M800720200.

73. Zhang, W., Jiang, H., Zhang, J., Zhang, Y., Liu, A., Zhao, Y., Zhu, X., Lin, Z., and Yuan, X. (2014). Liver X receptor activation induces apoptosis of melanoma cell through caspase pathway. Cancer Cell Int. *14*, 16. https://doi.org/10.1186/1475-2867-14-16.

74. Gan, X., Kaplan, R., Menke, J.G., MacNaul, K., Chen, Y., Sparrow, C.P., Zhou, G., Wright, S.D., and Cai, T.Q. (2001). Dual mechanisms of ABCA1 regulation by geranylgeranyl pyrophosphate. J. Biol. Chem. *276*, 48702–48708. https://doi.org/10.1074/jbc.M109402200.

75. Yeh, Y.-S., Goto, T., Takahashi, N., Egawa, K., Takahashi, H., Jheng, H.-F., Kim, Y.-I., and Kawada, T. (2016). Geranylgeranyl pyrophosphate performs as an endogenous regulator of adipocyte function via suppressing the LXR pathway. Biochem. Biophys. Res. Commun. *478*, 1317–1322. https://doi.org/10.1016/j.bbrc.2016.08.119.

76. Niemann, B., Haufs-Brusberg, S., Puetz, L., Feickert, M., Jaeckstein, M.Y., Hoffmann, A., Zurkovic, J., Heine, M., Trautmann, E.-M., Müller, C.E., et al. (2022). Apoptotic brown adipocytes enhance energy expenditure via extracellular inosine. Nature *609*, 361–368. https://doi.org/10.1038/s41586-022-05041-0.

77. Vila-Bedmar, R., Lorenzo, M., and Fernández-Veledo, S. (2010). Adenosine 5′-monophosphate-activated protein kinase-mammalian target of rapamycin cross talk regulates brown adipocyte differentiation. Endocrinology *151*, 980–992. https://doi.org/10.1210/en.2009-0810.

78. Labbé, S.M., Mouchiroud, M., Caron, A., Secco, B., Freinkman, E., Lamoureux, G., Gélinas, Y., Lecomte, R., Bossé, Y., Chimin, P., et al. (2016). mTORC1 is required for brown adipose tissue recruitment and metabolic adaptation to cold. Sci. Rep. *6*, 37223–37317. https://doi.org/10.1038/srep37223.

79. Gong, L., Xiao, Y., Xia, F., Wu, P., Zhao, T., Xie, S., Wang, R., Wen, Q., Zhou, W., Xu, H., et al. (2019). The mevalonate coordinates energy input and cell proliferation. Cell Death Dis. *10*, 327. https://doi.org/10.1038/s41419-019-1544-y.

80. Saci, A., Cantley, L.C., and Carpenter, C.L. (2011). Rac1 regulates the activity of mTORC1 and mTORC2 and controls cellular size. Mol. Cell *42*, 50–61. https://doi.org/10.1016/j.molcel.2011.03.017.

81. Kawada, T., Sakabe, S., Aoki, N., Watanabe, T., Higeta, K., Iwai, K., and Sugimoto, E. (1991). Intake of sweeteners and pungent ingredients increases the thermogenin content in brown adipose tissue of rat. J. Agric. Food Chem. *39*, 651–654. https://doi.org/10.1021/jf00004a004.

82. Irie, Y., Asano, A., Cañas, X., Nikami, H., Aizawa, S., and Saito, M. (1999). Immortal brown adipocytes from p53-knockout mice: differentiation and expression of uncoupling proteins. Biochem. Biophys. Res. Commun. *255*, 221–225. https://doi.org/10.1006/bbrc.1998.9999.

83. Kenmochi, M., Kawarasaki, S., Takizawa, S., Okamura, K., Goto, T., and Uchida, K. (2022). Involvement of mechano-sensitive Piezo1 channel in the differentiation of brown adipocytes. J. Physiol. Sci. *72*, 13. https://doi.org/10.1186/s12576-022-00837-1.

STAR★METHODS

KEY RESOURCES TABLE

REAGENT or RESOURCE	SOURCE	IDENTIFIER
Antibodies		
Rabbit polyclonal anti-UCP1, WB	Kawada et al.[81]	N/A
Rabbit polyclonal anti-β-Actin, WB	Cell Signaling	Cat#4967; RRID: AB_330288
Rabbit monoclonal anti-HMGCR, WB	Abcam	Cat# ab174830; RRID: AB_2749818
Rabbit monoclonal anti-RB, WB	Abcam	Cat# ab181616; RRID: AB_2848193
Rabbit polyclonal anti-C/EBPβ, WB	Santa Cruz Biotechnology	Cat# sc-150; RRID: AB_2260363
Rabbit polyclonal anti-C/EBPδ, WB	Santa Cruz Biotechnology	Cat# sc-636; RRID: AB_2078199
Rabbit polyclonal anti-α-Tubulin, WB	Cell Signaling	Cat# 2144; RRID: AB_2210548
Mouse monoclonal anti-Histone H3, WB	Cell Signaling	Cat# 3638; RRID: AB_1642229
Chicken polyclonal anti-MCT1, IF	Sigma-Aldrich	Cat# AB1286; RRID: AB_11212410
Rabbit monoclonal anti-PDGFRα, IF	Abcam	Cat# ab203491; RRID: AB_2892065
Goat polyclonal anti-Perilipin, IF	Novus Biologicals	Cat# NB100-60554; RRID: AB_922242
Rabbit polyclonal anti-Caspase 3, WB	GeneTex	Cat# GTX110543, RRID: AB_10722709
Rabbit polyclonal anti-Cleaved Caspase 3 (Asp175), WB	Cell Signaling	Cat# 9661; RRID: AB_2341188
Goat Anti-Mouse IgG - Horseradish Peroxidase conjugated	Santa Cruz Biotechnology	Cat# sc-2005; RRID: AB_631736
Goat Anti-Rabbit IgG - Horseradish Peroxidase conjugate	Novus Biologicals	Cat# NBP1-75297; RRID: AB_11033396
Goat Anti-Chicken IgY – CF488A conjugate	Biotium	Cat# 20020; RRID: AB_10559185
Donkey Anti-Rabbit IgG – CF568 conjugated	Biotium	Cat# 20098; RRID: AB_10557118
Donkey Anti-Goat IgG – CF568 conjugated	Biotium	Cat# 20106; RRID: AB_10559672
Chemicals, peptides, and recombinant proteins		
Lovastatin (LVS)	Tokyo Chemical Industry	CAS#75330-75-5
Atorvastatin calcium salt trihydrate (ATR)	Tokyo Chemical Industry	CAS#344423-98-9
Mevalonic acid lithium salt (MVA)	Sigma-Aldrich	CAS#150-97-0
Farnesyl pyrophosphate ammonium salt (FPP)	Sigma-Aldrich	CAS#13058-04-3
Geranylgeranylpyrophosphate triammonium salt (GGPP)	Sigma-Aldrich	CAS#6699-20-3
Squalene (SQ)	Nacalai Tesque	CAS#111-02-4
Zoledronic acid monohydrate (Zol)	Sigma-Aldrich	CAS#165800-06-6
GGTI-286	Cayman Chemical	CAS#171744-11-9
Ubiquinone	Tokyo Chemical Industry	CAS#303-98-0
Ubiquinol	Toronto Research Chemicals	CAS#992-78-9
Hoechst 33342	Nacalai Tesque	CAS#23491-52-3
Nile red	Tokyo Chemical Industry	CAS#7385-67-3
Dulbecco's modified Eagle medium (High Glucose)	Nacalai Tesque	Cat#08458-16
Fetal Bovine Serum	Gibco	Cat#10270106
Penicillin-Streptomycin Mixed Solution	Nacalai Tesque	Cat#26253-84
Dexamethasone (Dex)	Nacalai Tesque	CAS#50-02-2
3-Isobutyl-1-methylxanthine (IBMX)	Nacalai Tesque	CAS#28822-58-4
Insulin	Wako Pure Chemical	CAS#11061-68-0
3, 3′, 5′-Triiodo-L-thyronine (T_3)	Sigma-Aldrich	CAS#55-06-1
Indomethacin	Wako Pure Chemical	CAS#53-86-1

(*Continued on next page*)

Continued

REAGENT or RESOURCE	SOURCE	IDENTIFIER
Rosiglitazone	LKT Laboratories	CAS#122320-73-4
Isoproterenol (ISO)	Sigma-Aldrich	CAS#5984-95-2
CL-316,243	Sigma-Aldrich	CAS#138908-40-4
Tamoxifen	Tokyo Chemical Industry	CAS#54965-24-1
Corn oil	Nacalai Tesque	CAS#8001-30-7
Protease Inhibitor cocktail	Nacalai Tesque	Cat#03969-21
Phosphatase Inhibitor cocktail	Nacalai Tesque	Cat#07575-51
PhosSTOP phosphatase inhibitor cocktail	Roche	Cat#4906837001
Immobilon-P polyvinylidene fluoride transfer membrane	Millipore	Cat#IPVH00010
Blocking One Histo	Nacalai Tesque	Cat#06349-64
Fluoro-KEEPER Antifade Reagent, Non-Hardening Type with DAPI	Nacalai Tesque	Cat#12745-74
Hematoxylin	Merck	Cat#105174
EosinY	Nacalai Tesque	CAS#17372-87-1
QIAzol Lysis reagent	QIAGEN	Cat#79306
Sepasol Super-I	Nacalai Tesque	Cat#09379-84
Moloney murine leukemia virus reverse transcriptase	Promega	Cat#M170B
Proteinase K	Nacalai Tesque	CAS#39450-01-6
Phenol:chloroform:isoamyl alcohol (25:24:1)	Nacalai Tesque	Cat#25970-56
EmeraldAmp MAX PCR Master Mix	Takara	Cat#RR320B
THUNDERBIRD® SYBR® qPCR Mix	Toyobo	Cat#QPS-201
Immobilon Western Chemiluminescent HRP Substrate	Millipore	Cat#WBKLS0500
Triton X-100	Nacalai Tesque	CAS#9002-93-1
Critical commercial assays		
DC Protein Assay	Bio-Rad	Cat#5000112
Annexin V-FITC Apoptosis Detection Kit	Nacalai Tesque	Cat#15342-54
in situ Apoptosis Detection Kit	Takara	Cat#MK500
CellTiter-96® Aqueous One Cell Proliferation Assay (MTS assay)	Promega	Cat#G3581
Glucose C-test Kit	Wako Pure Chemical	Cat#997-03001
Cholesterol E-test Kit	Wako Pure Chemical	Cat#993-02501
Triacylglycerol E-test Kit	Wako Pure Chemical	Cat#290-63701
Experimental models: Cell lines		
Mouse: HB2	Irie et al.[82]	N/A
Mouse: immortalized pre-adipocytes isolated from interscapular BAT of UCP1-mRFP1 mice	Kenmochi et al.[83]	N/A
Experimental models: Organisms/strains		
Mouse: C57BL/6J	SLC, Japan	N/A
Mouse: C57BL/6N	SLC, Japan	N/A
Mouse: C57BL/6N-albino: B6N-Tyr$^{c\text{-}Brd}$/BrdCrCrl	Charles River Laboratories	RRID: IMSR_CRL:493
Mouse: Ctrl: Hmgcr$^{flox/flox}$	Yeh et al.[58]	N/A
Mouse: Ucp1-Cre: B6.FVB-Tg(Ucp1-cre)1Evdr/J	The Jackson Laboratory	RRID: IMSR_JAX:024670
Mouse: BAT KO: Hmgcr$^{flox/flox}$Ucp1-Cre	This paper	N/A
Mouse: Adipoq-CreER^{T2}: C57BL/6-Tg(Adipoq-cre/ERT2)1Soff/J	The Jackson Laboratory	RRID: IMSR_JAX:025124
Mouse: aiKO: Hmgcr$^{flox/flox}$Adipoq-CreER^{T2}	This paper	N/A
Mouse: UCP1-mRFP1: UCP1-mRFP1 BAC Tg	Kawarasaki et al.[41]	N/A

(*Continued on next page*)

Continued

REAGENT or RESOURCE	SOURCE	IDENTIFIER
Mouse: KK-A^{y}: KK.Cg-A^{y}/TaJcl	CLEA, Japan	RRID: MGI:3833283
Mouse: ICR	SLC, Japan	N/A
Oligonucleotides		
See Table S2	This paper	N/A
Software and algorithms		
ImageJ (version 1.8.0)	National Institutes of Health	https://imagej.nih.gov/ij/
SPSS Statistics (version 17.0)	IBM	https://www.ibm.com/products/spss-statistics
DP-BSW (version 3.2.1)	Olympus	https://www.olympus-lifescience.com/en/support/downloads/
i-control™ Microplate Reader Software	Tecan	https://lifesciences.tecan.com/plate_readers/infinite_200_pro?p=Software
FV10-ASW (version 4.2)	Olympus	https://www.olympus-lifescience.com/ja/support/downloads/
PMCapture Pro 6.0 software	Roper Technologies	N/A
Other		
Fluoview FV1000 Olympus IX81 Confocal Microscope	Olympus	N/A
Olympus IX83 microscope equipped with DP71 CCD camera	Olympus	N/A
Infinite® 200	Tecan	N/A
Bioruptor UCD-300	Cosmo Bio, Japan	N/A
ImageQuant LAS 4000	GE Healthcare	N/A
Light Cycler 480 II	Roche	N/A
MF	Oriental Yeast Co., Japan	N/A
Thermometer (BAT-7001H)	Physitemp Instruments Inc.	N/A
FLIR T335 infrared camera	Teledyne FLIR	N/A
Lumazone *in vivo* macro imaging system	Roper Technologies	N/A

RESOURCE AVAILABILITY

Lead contact

Further information and requests for resources and reagents should be directed to and will be fulfilled by the lead contact, Tsuyoshi Goto (goto.tsuyoshi.6x@kyoto-u.ac.jp).

Materials availability

Mouse line generated in this study will be available by the lead contact upon reasonable request.

Data and code availability

- Original western blot images and microscopy data reported in this paper will be available by the lead contact upon reasonable request.
- This paper does not report original code.
- Any additional information required to reanalyze the data reported in this paper is available from the lead contact upon request.

EXPERIMENTAL MODEL AND SUBJECT DETAILS

Mice

All animal experiments were performed according to protocols approved by the Animal Research Committee of Kyoto University, Kyoto, Japan (permission number: R2-50). All mice were housed at 24 ± 1°C and

maintained under a 12 h light/dark cycle. During all experiments, mice were fed a normal chow diet (MF; Oriental Yeast Co., Japan). To achieve LVS-induced pharmacological inhibition of the MVA pathway in the fetus, male UCP1-mRFP1 BAC Tg mice[41] were mated with C57BL/6N-albino female mice (B6N-Tyr$^{c\text{-}Brd}$/BrdCrCrl; Charles River Laboratories). Female mice with confirmed virginal plug the day after mating were subcutaneously administered 10 mg/kg/day of LVS (Tokyo Chemical Industry) from embryonic day 8.5 (E8.5) to 18.5 (E18.5) (11 days in total). The mRFP1-positive offspring were identified by genotyping and analyzed on postnatal day 0.5 (P0.5). BAT-specific *Hmgcr* KO mice were generated by crossing *Hmgcr*$^{flox/flox}$ mice[58] with *Ucp1-Cre* mice (B6.FVB-Tg [Ucp1-cre] 1Evdr/J; The Jackson Laboratory) to generate *Hmgcr*$^{flox/+}$*Ucp1-Cre* progeny. The progeny was then backcrossed with *Hmgcr*$^{flox/flox}$ mice, and their *Hmgcr*$^{flox/flox}$*Ucp1-Cre* progeny were backcrossed with *Hmgcr*$^{flox/flox}$ mice to yield *Hmgcr*$^{flox/flox}$ and *Hmgcr*$^{flox/flox}$*Ucp1-Cre* progeny. *Hmgcr*$^{flox/flox}$ mice were used as the controls. To generate tamoxifen-inducible adipocyte-specific *Hmgcr* knockout (aiKO) mice, *Hmgcr*$^{flox/flox}$ mice were mated with *Adipoq-Cre*ER^{T2} mice (C57BL/6-Tg [Adipoq-cre/ERT2] 1Soff/J; The Jackson Laboratory). The progeny of *Hmgcr*$^{flox/flox}$*Adipoq-Cre*ER^{T2} mice were obtained in the same manner as *Hmgcr*$^{flox/flox}$*Ucp1-Cre* mice. 13-week-old male *Hmgcr*$^{flox/flox}$*Adipoq-Cre*ER^{T2} mice were intraperitoneally injected with tamoxifen (100 mg/kg/day; Tokyo Chemical Industry) or corn oil (Nacalai Tesque) for 5 consecutive days. Twenty days after the tamoxifen injection, the mice were sacrificed with isoflurane for further investigation. For the ATR treatment experiment, 4-week-old male KK-*A*^{y} mice (KK.Cg-*A*^{y}/TaJcl; CLEA, Japan) were intraperitoneally injected with ATR (10 mg/kg/day; Tokyo Chemical Industry) for 52 consecutive days. The mice were sacrificed using isoflurane for further investigation.

HB2 cells

HB2 preadipocytes from the interscapular fat of p53-KO mice were cultured as described previously[82] with some modifications. Briefly, HB2 cells were maintained in Dulbecco's modified Eagle medium (Nacalai Tesque) with 10% fetal bovine serum (Gibco) and 100 U/mL penicillin and 100 μg/mL streptomycin (Nacalai Tesque) at 37°C in 5% CO_2. Post-confluent HB2 cells were incubated in a differentiation medium containing 1 μM dexamethasone (DEX; Nacalai Tesque) and 0.5 mM 3-isobutyl-1-methylxanthine (IBMX; Nacalai Tesque) in the growth medium. After 48 h, the cell culture medium was replaced with a post-differentiation medium containing 10 μg/mL insulin (Wako Pure Chemical) and 50 nM 3,3,5-triiodothyronine (T_3; Sigma-Aldrich) in the growth medium, and the medium was changed every two days. To determine the effect of the MVA pathway on brown adipocyte differentiation, post-confluent HB2 brown preadipocytes were treated with LVS (Tokyo Chemical Industry), ATR (Tokyo Chemical Industry), LVS in combination with metabolites from the MVA pathway (MVA, FPP, and GGPP, Sigma-Aldrich; SQ, Nacalai Tesque), Zol (Sigma-Aldrich), Zol in combination with GGPP, LVS in combination with coenzyme Q_{10} (Ubiquinone, Tokyo Chemical Industry; Ubiquinol, Toronto Research Chemicals), GGTI-286 (Cayman Chemical), or GGTI-286 in combination with GGPP until day 2 after the induction of differentiation. On day 4, the HB2 cells were harvested for subsequent experiments. For DNA and intracellular lipid staining, brown adipocytes were double-stained with 5 μg/mL Nile red (Tokyo Chemical Industry) and 5 μg/mL Hoechst 33342 (Nacalai Tesque). The cells treated with Nile red and Hoechst 33342 were observed under a fluorescence microscope (Olympus IX83; Olympus), and images were captured with a DP71 CCD camera (Olympus). Fluorescence images were collected and merged by using DP-BSW software (Olympus). The fluorescence intensities were measured (Nile red, 485 nm/535 nm; Hoechst 33342, 360 nm/465 nm) by an Infinite® 200 apparatus (Tecan) and analyzed using i-control™ Microplate Reader Software (Tecan). For the LVS treatment experiment with mature brown adipocytes, differentiation-induced mature HB2 cells were treated with LVS, LVS in combination with metabolites from the MVA pathway, Zol, Zol in combination with GGPP, coenzyme Q_{10}, or GGTI-286 from day 4 to day 8. On day 8, the HB2 cells were harvested for subsequent experiments. For the ISO treatment experiments, differentiation-induced HB2 cells were stimulated with 1 μM ISO (Sigma-Aldrich) for the indicated time durations, as described in Figure 1F and harvested for further analysis. Apoptotic cells were detected by using the Annexin V-FITC Apoptosis Detection Kit (Nacalai Tesque) according to the manufacturer's instructions, and cells stained by both Annexin V-FITC and PI were observed under a fluorescence microscope (Olympus IX83; Olympus). Fluorescence images were captured, collected, and merged as mentioned above. Cell viability was measured by using CellTiter-96® Aqueous One Cell Proliferation Assay (MTS assay; Promega) in accordance with the manufacturer's instructions.

Primary brown preadipocytes

Immortalized brown preadipocytes from interscapular BAT of UCP1-mRFP1 transgenic mice were cultured as described previously.[83] Briefly, post-confluent immortalized primary cells were incubated in a differentiation medium containing 0.25 μM DEX (Nacalai Tesque), 0.5 mM IBMX (Nacalai Tesque), 1 nM T_3 (Sigma-Aldrich), 10 μg/mL insulin (Wako Pure Chemical), 125 μM indomethacin (Wako Pure Chemical), and 0.5 μM rosiglitazone (LKT Laboratories) in the growth medium. After 48 h, the cell culture medium was replaced with a post-differentiation medium containing 5 μg/mL insulin (Wako Pure Chemical), 1 nM T_3 (Sigma-Aldrich), and 0.5 μM rosiglitazone (LKT Laboratories) in the growth medium, and the medium was changed every two days. For the ISO treatment experiments, differentiation-induced brown adipocytes were stimulated with 1 μM ISO (Sigma-Aldrich) for the indicated time durations, as described in Figures S1A and S1C and harvested for further analysis.

METHOD DETAILS

RNA preparation and quantification of gene expression

Total RNA was extracted using the QIAzol Lysis reagent (QIAGEN) or Sepasol Super-I (Nacalai Tesque), and 2 μg of total RNA samples was reverse-transcribed using Moloney murine leukemia virus reverse transcriptase (Promega), according to the manufacturer's instructions, in a thermal cycler. To quantify mRNA expression levels, quantitative reverse transcription-polymerase chain reaction was performed using a Light Cycler 480 II System (Roche) with THUNDERBIRD® SYBR® qPCR Mix (Toyobo). All measured mRNA expression levels were normalized to ribosomal protein lateral stalk subunit P0 (*Rplp0*) expression levels. The primer sequences are provided in Table S2.

Protein extraction

For whole cell lysates, the cells were washed twice with ice-cold PBS, and lysed in ice-cold lysis buffer (50 mM Tris-HCl pH 7.4, 150 mM NaCl, 1% Triton X-100 [v/v], 0.25% deoxycholate [w/v], 0.1% sodium dodecyl sulfate [SDS; w/v], and 1 mM EDTA) supplemented with 1% protease inhibitor cocktail (Nacalai Tesque) and 1% phosphatase inhibitor cocktail (Nacalai Tesque). After centrifugation at 16,700 ×*g* for 10 min at 4°C, the resulting supernatant was quantified using a DC protein assay Kit (Bio-Rad) according to the manufacturer's instructions. Samples were denatured by boiling for 5 min in Laemmli sample buffer and used for western blotting analysis. For BAT lysates, BAT was homogenized and lysed in ice-cold lysis buffer (78 mM Tris-HCl pH 6.8, 6.25% sucrose [w/v], and 2% SDS [w/v]) supplemented with 1% protease inhibitor cocktail (Nacalai Tesque) and PhosSTOP phosphatase inhibitor cocktail (Roche). After centrifugation at 21,500 ×*g* for 30 min at room temperature, the resulting supernatant was quantified and denatured as mentioned above.

Subcellular fractionation

Cells were washed twice with ice-cold PBS, harvested, and lysed in ice-cold lysis buffer (10 mM HEPES pH 7.9, 10 mM KCl, 1.5 mM MgCl2, 0.1% Triton X-100 [v/v], 0.1 mM EDTA and 1 mM dithiothreitol) supplemented with 1% protease inhibitor cocktail (Nacalai Tesque) and PhosSTOP phosphatase inhibitor cocktail (Roche) and incubated on ice for 15 min. The lysates were centrifuged at 860 ×*g* for 5 min at 4°C to isolate nuclei. The cytoplasm-containing supernatants were transferred to new tubes and centrifuged at 13,800 ×*g* for 1 h at 4°C to remove any contaminating nuclei. The supernatants were collected as cytoplasmic fractions. The nuclei pellets were resuspended in high salt buffer (20 mM HEPES pH 7.9, 400 mM KCl, 1.5 mM MgCl2, 1% nonidet P-40 [v/v], 0.1 mM EDTA, 10% glycerol [v/v] and 1 mM dithiothreitol) supplemented with protease inhibitor and phosphatase inhibitor as mentioned above, followed by sonication with a Bioruptor UCD-300 (Cosmo Bio). The suspension was centrifuged at 16,200 ×*g* for 5 min at 4°C and supernatants were collected as nuclear fractions. Protein quantification was performed using a DC protein assay Kit (Bio-Rad) according to the manufacturer's instructions. Samples were denatured by boiling for 5 min in Laemmli sample buffer, and used for western blotting analysis.

Western blotting

Protein samples were separated by SDS-PAGE and transferred to an Immobilon-P polyvinylidene fluoride transfer membrane (Millipore). After blocking, the membrane was incubated with a primary antibody overnight at 4°C, followed by incubation with the horseradish peroxidase-conjugated secondary antibody (HRP-conjugated goat anti-mouse IgG, Santa Cruz Biotechnology; HRP-conjugated goat anti-rabbit IgG, Novus Biologicals). Primary antibodies used in this study were anti-UCP1 (an antiserum from a rabbit

immunized with the rat UCP1 purified from BAT in cold-exposed rats, as described previously[81]), anti-β-Actin (4967; Cell Signaling), anti-HMGCR (ab174830; Abcam), anti-RB (ab181616; Abcam), anti-C/EBPβ (sc-150; Santa Cruz Biotechnology), anti-C/EBPδ (sc-636; Santa Cruz Biotechnology), anti-α-Tubulin (2144; Cell Signaling), anti-Histone H3 (3638; Cell Signaling), anti-Caspase 3 (GTX110543; GeneTex), and anti-Cleaved Caspase 3 (Asp175) (9661; Cell Signaling). Proteins were visualized by chemiluminescence using an Immobilon Western Chemiluminescent HRP Substrate (Millipore). The chemiluminescent signal was detected using an ImageQuant LAS4000 (GE Healthcare) apparatus. The intensity of Western blot bands was quantified with ImageJ software (National Institutes of Health).

Thermal imaging and *in vivo* fluorescence imaging of neonates

Neonates (P0.5) were removed from the cage and the warmest spot within a defined region in the upper dorsal area of each neonatal mouse was identified by infrared thermographic camera (T335; Teledyne FLIR) (Figure 4G). Fluorescence imaging was performed in the interscapular area using a Lumazone *in vivo* macro imaging system (Roper Technologies). Bright field and fluorescence imaging (excitation filter, 530–560 nm; emission filter, 590–650 nm) were performed with 0.3 s exposure time (Figure 4E). Surface plots of the images were acquired using PMCapture Pro 6.0 software (Roper Technologies). The range of the surface plot was 50–180 relative fluorescence units (Figure 4E). Fluorescence intensity was calculated using the ImageJ software (National Institutes of Health).

Rectal temperature measurement

For cold exposure experiments shown in Figures 1B and 1D, 14-week-old male C57BL/6N mice (SLC, Japan) were housed individually and exposed to 10°C with *ad libitum* food and water. The mice were anesthetized with isoflurane at the indicated time points and dissected for further analysis. For cold exposure experiments shown in Figure 7I, 3-h-fasted 11–12-week-old male BAT KO and their littermates (Ctrl) were placed individually in cages and exposed to 4°C with free access to water. The rectal temperature was measured with a thermometer (BAT7001H; Physitemp Instruments Inc.) before exposure to cold and every hour after cold exposure. Infrared thermal images were obtained before and 3 h after cold exposure at 6°C using an infrared thermographic camera (T335; FLIR) (Figure 7J). For the CL316,243 injection experiment (Figure 7K), 11–12-week-old male BAT KO mice and Ctrl mice were anesthetized with isoflurane at concentrations of 1.5%, were placed on a heat block set at 38.5°C. In addition, mice were subcutaneously administered saline or CL316,243 (1 mg/kg; Sigma-Aldrich) after a stable rectal temperature was confirmed; then, rectal temperature was monitored every minute using a thermometer (BAT7001H; Physitemp Instruments Inc.).

Hematoxylin and eosin staining of tissue sections

BAT was fixed with Bouin's solution (saturated picric acid: 37% formaldehyde: glacial acetic acid = 15 : 5: 1) for 3 h, embedded in paraffin, and sectioned at 5 μm thickness using a microtome. The sections were transferred onto silane coated slides, deparaffinized with xylene, and rehydrated with sequential washes with diluted ethanol (100%, 99%, 90%, and 80%) followed by washing with running water. The samples were stained with eosin Y (Nacalai Tesque) and counterstained with Gill's hematoxylin (Merck).

Immunostaining analysis of BAT

For immunofluorescence staining with MCT1 and PDGFRα, deparaffinized BAT sections were incubated in 0.3% Triton X-100 (Nacalai Tesque)/PBS for 1 h, blocked with Blocking One Histo (Nacalai Tesque) for 10 min, and incubated with the primary antibodies diluted with Blocking One Histo (Nacalai Tesque) overnight at 4°C. After washing three times with PBS, the sections were incubated with fluorescence-conjugated secondary antibodies for 2 h. All sections were mounted with Fluoro-KEEPER Antifade Reagent with DAPI (Nacalai Tesque) and observed under a confocal microscope (FluoView FV1000 Olympus IX81; Olympus). Fluorescence images were obtained and merged by using FV10-ASW software (Olympus). Primary antibodies used for immunofluorescence staining included anti-MCT1 (AB1286; Sigma-Aldrich), anti-PDGFRα (ab203491; Abcam). Secondary antibodies used for immunohistochemical staining were as follows: CF488A-labeled goat anti-chicken IgY (Biotium), and CF568-labeled donkey anti-rabbit IgG (Biotium).

TUNEL staining of BAT section

TUNEL staining was performed using the *in situ* Apoptosis Detection Kit (Takara) following the manufacturer's instructions. Briefly, deparaffinized BAT sections were incubated in proteinase K (Nacalai Tesque) containing solution (50 mM Tris-HCl pH8.0, 1 mM EDTA, and 20 μg/mL proteinase K) for 10 min, washed with PBS, blocked with Blocking One Histo (Nacalai Tesque) for 10 min, and incubated with anti-Perilipin (NB100-60554; Novus Biologicals) diluted with Blocking One Histo (Nacalai Tesque) overnight at 4°C. After washing three times with PBS, the sections were incubated with CF568-labeled donkey anti-goat IgG (Biotium) and TUNEL labeling buffer for 90 min at 37°C. After washing three times with PBS, all sections were mounted with Fluoro-KEEPER Antifade Reagent with DAPI (Nacalai Tesque) and observed under a confocal microscope (FluoView FV1000 Olympus IX81; Olympus).

Triglyceride measurement

HB2 cells were washed twice with ice-cold PBS, lysed in 0.5% Triton X-100 (Nacalai Tesque)/PBS, and sonicated by Bioruptor UCD-300 (Cosmo Bio, Japan) at a maximum setting for 30 s, performed four times on ice. The sonicated samples were boiled for 10 min and centrifuged at 16,200 × *g* for 10 min at 4°C. The supernatant was collected, and the triglyceride concentration was measured using a Triglyceride E-test Kit (Wako Pure Chemical) in accordance with the manufacturer's instructions.

Mouse genotyping

mRFP1-positive mice and BAT-specific *Hmgcr* KO mice were identified by genotyping, as described previously.[58] Briefly, the tail (2–3 mm) of mice or tissues were incubated with a lysis buffer (10 mM Tris-HCl pH 8.0, 25 mM EDTA, 0.5% SDS, and 100 mM NaCl) containing 1 mg/mL proteinase K (Nacalai Tesque) at 50°C overnight. After the samples were dissolved, 200 μL of phenol:chloroform:isoamyl alcohol (25:24:1; Nacalai Tesque) was added, and centrifuged at 13,800 × *g* for 5 min at 4°C. The supernatant was transferred to a new tube, and 200 μL of chloroform was added. After centrifugation at 14,000 × *g* for 5 min at 4°C, 160 μL of the supernatant was transferred to new tube containing 16 μL of 3 M Na-acetate and 400 μL of ethanol and centrifuged at 19,000 × *g* for 20 min at 4°C. The DNA pellet was dissolved in TE buffer (pH 8.0). Genomic DNA was amplified using EmeraldAmp MAX PCR Master Mix (Takara) in a thermal cycler and confirmed by agarose gel electrophoresis. Primer sequences used are listed in Table S2.

Analysis of plasma chemical parameters

Levels of plasma glucose, cholesterol, and triacylglycerol were measured by using Glucose C-test Kit (Wako Pure Chemical), Cholesterol E-test Kit (Wako Pure Chemical), and Triacylglycerol E-test Kit (Wako Pure Chemical), respectively, in accordance with the manufacturer's instructions.

Transfer C57BL/6N neonates to ICR mice

On postnatal day 0.5 (P0.5), the neonates from the Veh or LVS (sc., 10 mg/kg/day from embryonic day E8.5 to embryonic day E18.5)-treated C57BL/6N mice (SLC, Japan) were removed from their dams and transferred to lactating ICR mice (SLC, Japan) within 24 h to be fostered. The number of neonates to be fostered per ICR mouse (fostering mouse) was limited to 5–6 to minimize the variability in pup weaning weight. ICR mice were used to foster neonates until weaning. The pups were weaned from the dam at 21 days of age and fed a normal chow diet (MF; Oriental Yeast Co., Japan) throughout the experimental period. Among grown-up mice, 9-week-old female mice were used in the experiments.

QUANTIFICATION AND STATISTICAL ANALYSIS

Data are presented as the mean ± standard error of the mean (SEM). Statistical analysis was performed using unpaired two-tailed Student's t test or one-way analysis of variance (ANOVA) followed by Tukey's HSD post hoc test. Correlation was analyzed by Pearson's correlation. Differences were considered statistically significant at $p < 0.05$. Statistical differences are indicated as *$p < 0.05$, **$p < 0.01$, ***$p < 0.001$. Analyses were performed using SPSS Statistics for Windows, Version 17.0 (IBM).